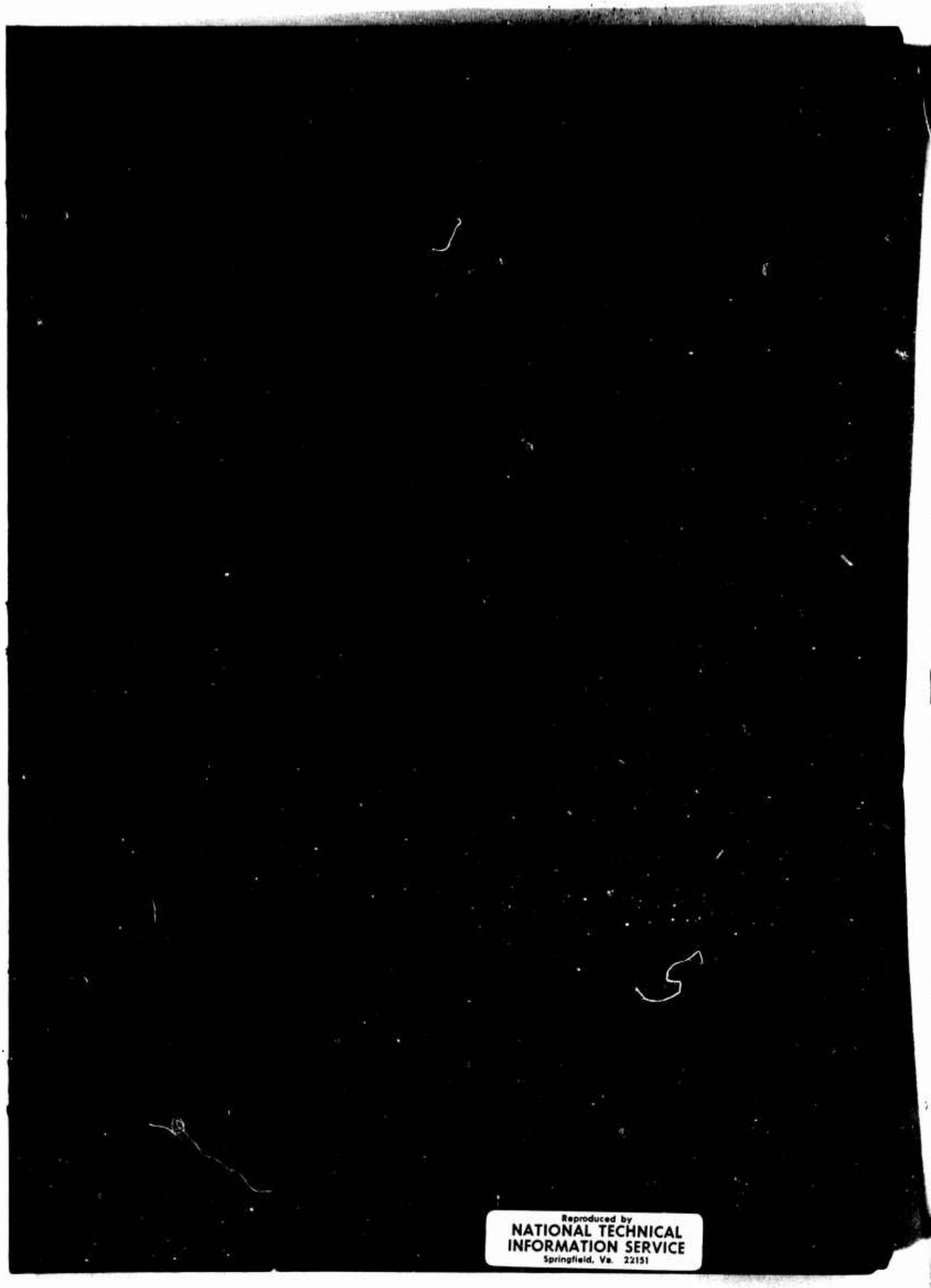

UNCLASSIFIED

Security Classification

DOCUMENT CONTROL DATA - R & D

(Security classification of title, body of abstract and indexing annotation must be entered when the overall report is classified)

1 ORIGINATING ACTIVITY (Corporate author)	2a. REPORT SECURITY CLASSIFICATION
ROCHESTER APPLIED SCIENCE ASSOCIATES, INC. 140 Allens Creek Road Rochester, New York 14618	UNCLASSIFIED 2b. GROUP N/A

3 REPORT TITLE

AN EXPERIMENTAL STUDY OF TIP VORTEX MODIFICATION BY MASS FLOW INJECTION

4 DESCRIPTIVE NOTES *(Type of report and inclusive dates)*

FINAL TECHNICAL REPORT - 1 February 1969 - 31 January 1971

5 AUTHOR(S) *(First name, middle initial, last name)*

Stephen A. Rinehart; John C. Balcerak; Richard P. White, Jr.

6 REPORT DATE	7a. TOTAL NO OF PAGES	7b. NO OF REFS
January 1971	75	5

8a. CONTRACT OR GRANT NO.	9a. ORIGINATOR'S REPORT NUMBER(S)
N00014-69-C-0169 b. PROJECT NO	71-01
c.	9b. OTHER REPORT NO(S) *(Any other numbers that may be assigned this report)*
d.	

10 DISTRIBUTION STATEMENT

Approved for public release; distribution unlimited

11 SUPPLEMENTARY NOTES	12. SPONSORING MILITARY ACTIVITY
	Office of Naval Research Aeronautics Code 461 Arlington, Virginia 22217

13. ABSTRACT

An experimental program was conducted to investigate the modifications of a tip vortex which could be obtained by injecting the core of a tip vortex with a stream of air. Wind tunnel tests of an airfoil model were conducted at the Naval Ship Research and Development Center during October and November, 1970.

The results obtained from flow-visualization studies, balance data, and vortex-meter measurements show ~~that~~ the strength of the tip vortex can be reduced significantly by the injection of a linear mass flow of air into the core of the tip vortex. Also, the results from the balance data show that the mean value of the lift force did not change with the reduction in strength of the tip vortex. The results also indicate that the jet flow did not interact significantly with wing flow and, thus, the change noted in the drag force was obtained by "jet thrust". The reduction in drag obtained with injection is important since it allows the recovery of power required to inject the tip vortex core with mass flow. (U)

DD FORM 1 NOV 65 1473

UNCLASSIFIED

Security Classification

14 KEY WORDS	LINK A		LINK B		LINK C	
	ROLE	WT	ROLE	WT	ROLE	WT
Aerodynamics						
Rotor Blades						
Tip Vortex						
Viscous Mixing						
Swirling Flow						
Mass Flow Injection						

RASA REPORT 71-01

AN EXPERIMENTAL STUDY OF TIP VORTEX MODIFICATION BY MASS FLOW INJECTION

FINAL TECHNICAL REPORT For the Period
1 February 1969 - 31 January 1971

by

Stephen A. Rinehart
John C. Balcerak
Richard P. White, Jr.

Prepared under Contract No. N00014-69-C-0169
Req. No. NR 212-194/12-16-69 (Code 461)
by
ROCHESTER APPLIED SCIENCE ASSOCIATES, INC.
140 Allens Creek Road, Rochester, New York 14618
716/271-3450

for

OFFICE OF NAVAL RESEARCH
AERONAUTICS, CODE 461
DEPARTMENT OF THE NAVY
Arlington, Virginia 22217

ACKNOWLEDGMENTS

The authors wish to express their appreciation to Mr. Robert Polvino who assisted in conducting the experiment and to Mr. Lawrence Sutton for his help in data reduction.

ABSTRACT

An experimental program was conducted to investigate the modifications of a tip vortex's characteristics which could be obtained by injecting the core of the vortex with a stream of air. Wind tunnel tests of an airfoil model were conducted at the Naval Ship Research and Development Center during October and November, 1970.

The results obtained from flow visualization studies, balance data, and vortex-meter measurements show that the concentrated vorticity associated with the trailing tip vortex can be significantly dissipated in the near flow field (i.e., within six and one-half chordlengths) by chordwise injection of air into the core of the tip vortex. The results from balance data show that the mean value of the total model lift force did not change under the mass injection rates considered. The changes occurring in the total drag force were obtained solely by thrust of the nozzle. The reduction in total drag force obtained by mass injection of the core is significant since it would allow the recovery of power required to inject a tip vortex core in practical applications.

TABLE OF CONTENTS

LIST OF SYMBOLS

L = Total lift as measured and read on scales of balance system, lb

L_N = Net lift on model, i.e., L minus tare due to jet thrust, lb

D = Total drag as measured and read on scales of balance system, lb

D_N = Net drag on model, i.e., D minus tare due to jet thrust, lb

m_i = Injected mass flow rate, lb/sec

R = Total roll moment as measured and read on scales of balance system, ft-lb

P_N = Net roll moment on model, i.e., R minus tare due to jet thrust, ft-lb

P = Total pitching moment as measured and read on scales of balance system, ft-lb

P_N = Net pitching moment on model, i.e., P minus tare due to jet thrust, ft-lb

V = Free-stream speed, ft/sec

α = Model angle of attack, degrees

ζ = Vorticity associated with tip vortex core, rad/sec

ρ = Free-stream mass density

ϕ_c = Swirl angle

LIST OF TABLES

LIST OF FIGURES

LIST OF FIGURES

LIST OF FIGURES

LIST OF FIGURES

I. INTRODUCTION

Any airfoil in flight generates a system of trailing vortices as a result of the variation in lift along the span. The trailing vortex sheet shed by an airfoil tends to roll up quickly to form a pair of discrete vortex filaments. In particular, the trailing wake at some distance behind a rotor blade or wing will consist of a root and a tip vortex. The free edge of the vortex sheet curls over, under the influence of the induced velocity field of the sheet, and takes the form of a spiral, as depicted in Figure 1.

The roll-up of the vortex sheet into a concentrated core presents a problem which is very important to helicopter aerodynamic, dynamic and acoustic analysis since it has been observed that rotor blades often pass through or near each other's wake causing extremely high local induced angles of attack. As a result of the rapid change in angle of attack when a rotor passes in the neighborhood of a vortex filament, rapid changes in lift occur which produce an impulsive dipole-type noise. The intensity of this impulsive noise is dependent upon: a) the interaction length along the span of the rotor, b) the strength and velocity distribution of the vortex filament, c) the rotor velocity, d) the distance that the blade chord passes from the vortex filament, and e) the alignment of the rotor with the filament at the time of interaction.

Various research efforts have been conducted by investigators to modify the tip vortex beneficially without destroying the performance characteristics of the aircraft by eliminating the problem at its source. Various degrees of success have been obtained in this research area in the last few years. Notable among these efforts have been those conducted by Spencer, Sternfeld, and McCormick on swept and porous tips (Ref. 1)

and Tanner of Bell on the twisted-swept tip (Ref. 2). While these approaches had well-founded technical bases, they were generally impractical because of performance penalties or because of difficulties in adapting the requisite modifications to full-scale hardware operating in a realistic environment, possibly due to full-scale Reynolds number effects.

During a recent contract conducted by Rochester Applied Science Associates for the Office of Naval Research, under contract number N00014-69-C-0169 (Ref. 3), it was determined theoretically that significant beneficial modifications of the tip vortex core size, axial and swirl velocity distributions, and tip vortex strength could be achieved by injecting an airstream into the core of the tip vortex. Since the results of the theoretical investigation were encouraging, the present experimental program was conducted to see if the results of the theory could be substantiated. The test program, conducted in November 1970 in the 7-by-10 foot low-speed wind tunnel at NSRDC, used a fixed-wing model. Air was injected from the wing model tip in a chordwise direction into the forming tip vortex core. The objective of the experimental program was to investigate the effects of angle of attack, dynamic pressure, and injected mass flow on the characteristics of the trailed tip vortex.

II. DESCRIPTION OF MODEL, WIND TUNNEL INSTALLATION AND INSTRUMENTATION

The model tested in this program was a straight, untapered NACA 0015 airfoil section with a chordlength of 8 inches, and a nominal semispan of 30 inches. The model was machined from a bar of 24S-T aluminum stock, and a 5/8-inch diameter hole was drilled through its span. The hole was centered at the mean line of the symmetrical section and the 15 percent chordline. At the root of the model, the hole at the 15 percent chord was plugged and another hole of the same diameter was drilled at a 15-degree angle from the 25 percent chord toward the leading edge to provide for the passage of the injected air supply. This arrangement allowed for the mounting of the quarter chord of the model at the center of the vertical axis of the wind tunnel balance system, and also allowed the exit nozzle for the injected air to be positioned as far forward as the quarter chord at the tip of the model. A 1-inch spanwise slot was milled from approximately the quarter chord of the model to its trailing edge, and to the depth of the chord centerline. The section between the slot and the 5/8-inch diameter hole was milled out to provide a cross sectional area of the exit nozzle equivalent to that of the 5/8-inch diameter hole. The outboard section of the slot and nozzle was formed by removable end caps. Square or half-airfoil shaped (planform view) end caps were fabricated, and by the exit nozzle could be positioned effectively inboard by using the square end caps as spacers. A cover plate could be installed over the entire slot to provide an essentially unmodified airfoil section. A close-up photograph of the exit nozzle and slot is shown in Figure 2, and a top view of the slot with the half-airfoil shaped end caps is shown in Figure 3. A schematic view of the model is shown in Figure 4.

The model was attached to a 5/8-inch thick, 8-inch diameter steel base plate by means of a tenon and mortise joint between the model root and baseplate. The baseplate, was bolted to a

strut, which in turn, was attached to the balance system of the wind tunnel. The strut provided for angle of attack control of the model during wind tunnel tests. The angle of attack of the model with respect to the geometric centerline of the tunnel was monitored by means of a mechanical counter. The injection-air supply was channeled from a "house" line through the strut to the base of the model, and the mass flow of the injected air was monitored by means of a venturi between the "house" line and the model. The only instrumentation on the model consisted of two differential pressure transducers positioned at the quarter chord and at approximately the 50 percent and 97 percent span.

Other instrumentation consisted of two hot-wire probes and an AEA Vortex Meter.[1] The hot-wire probes were mounted vertically from longitudinal arms attached to a swivel whose center was positioned 4 chordlengths (32 inches) behind the trailing edge of the model, and at the tunnel centerline. Provision was made for vertical traverse of the swivel assembly by means of a slide whose height was monitored manually by means of a graduated scale. The rotational position of the swivel was monitored from the output signal of a potentiometer which was attached to the lower end of the swivel. The longitudinal arms which were attached to the swivel were adjustable so that the forward hot-wire probe could be positioned from 0.5 to 2.5 chordlengths aft of the model trailing edge, and the rear hot-wire probe could be positioned from 5.5 to 7.5 chordlengths aft of the model trailing edge.

The vortex meter was attached to a three-component traverse mechanism which, in turn, was mounted on the tunnel floor aft of the model and off the tunnel centerline. The traverse mechanism provided for the measurement of vorticity in the range from 1.5 to 6.5 chordlengths behind the trailing edge of the model; approximately ±3 inches normal to the chordline; and

[1]Aero Engineering Associates, State College, Pennsylvania.

from approximately the 25 percent span position to approximately 3 inches outboard of the model tip. The position of the vortex meter in each direction was monitored manually by means of mechanical counters.

The output signals from the hot-wire probes, the pressure transducers and the potentiometer were recorded on a Visicorder, and the output signal from the vortex meter was monitored on an electronic counter.

During initial tests, a tuft mattress with a 1-inch grid was installed approximately 6-3/4 chordlengths aft of the trailing edge of the model in order to visualize the tip vortices for the various angle of attack and air-injection configurations. A camera was installed in the diffuser section of the wind tunnel in order to photograph the tuft pattern for the various configurations. A photograph showing the installation of the various appurtenances in the wind tunnel is shown as Figure 5.

Flow visualization tests were also conducted in conjunction with Sage Action, Inc., using a helium-bubble technique (Ref. 4) which is described in the report cited. These tests were arranged late in the program for a fortuitous schedule involving the program described herein, and one involving SAI, also under ONR sponsorship. For these flow visualization studies, the head from which the helium-filled bubbles are generated was positioned approximately 15 chordlengths upstream of the model, and on the longitudinal centerline of the tunnel. Its vertical position was aligned approximately with the injection slot at the tip of the model. The light source which illuminated the bubbles was positioned approximately 15 chordlengths downsteam of the model, and was aligned such that the center of the light beam illuminated the injection slot.

Photographs of the bubbles were taken from two positions; from the tunnel wall and ceiling. The former position was situated on the vacuum side of the model surface, and approximately 3 chordlengths downstream of the trailing edge of the

model. Photos of the flow field from this camera position were taken near the model and approximately 12 chordlengths downstream of the model. The ceiling camera was mounted approximately 6 chordlengths downstream of the model and near the tunnel centerline. Photos of the flow field from this position were taken only near the model. A schematic diagram of the set-up for these flow-visualization tests is shown in Figure 6.

III. WIND TUNNEL TESTS

Wind tunnel tests under this program were conducted in two phases. In the first phase, flow-visualization studies were conducted using a tuft mattress, hand-held tufts and smoke tests in the No. 2 (South) 7-by-10-foot Wind Tunnel at NSRDC. The remaining tests, which comprised the majority of the wind tunnel program, were conducted in the No. 1 (North) 7-by-10-foot Wind Tunnel at the same facility.

The former tests were conducted primarily to verify that a beneficial effect as regards modification of the tip vortex could be obtained with the design and location of the jet nozzle. If not, modification of the jet nozzle would have been attempted to obtain the anticipated result. The installation of the model in the South Tunnel could also be accomplished rather easily, and this arrangement would have precluded a second somewhat more difficult installation of the model in the North Tunnel if the preliminary tests were unsuccessful.

As it were, however, the initial set of wind tunnel tests proved to be quite successful, as it could be observed visually that the area of influence of the tip vortex, as indicated by the swirl pattern on the tuft mattress, could be reduced in size and intensity as the air-injection rate was increased. It is noted that because of the coarseness of the tuft grid (1-inch squares), it was found difficult to establish the precise air-injection rate required to significantly reduce the swirl pattern of the tip vortex on the tuft grid of any angle of attack. Another conclusion based on these tests was that air was being injected into the tip vortex more efficiently at lower angles of attack, which accounted for the more beneficial results. It was felt that more efficiency could be achieved at higher angles of attack by the placement of spacers between the injection slot

and the end cap of the model, which would effectively move the injection slot inboard. This arrangement was tested initially during the second series of tests in the North Wind Tunnel using similar visualization techniques, but it was observed that, in fact, the results were less beneficial.

Smoke tests conducted during the initial tunnel entry were rather disappointing, as control of the density of the smoke, in particular, proved to be difficult because of problems encountered with maintaining a constant temperature at the heated tip of the smoke probe. The usual problem of smoke accumulation in the tunnel was also present and compounded the minor mechanical and photographic difficulties. In spite of these difficulties, the smoke tests also indicated an increasing diffusion of the tip vortex with increasing mass injection rates.

Following the initial set of tests in the North Wind Tunnel which indicated that a slot near the model tip was most suitable of the configurations at hand, photographs were taken of the tuft mattress at a tunnel velocity of 100 fps for various angles of attack and mass injection rates. The tuft mattress was removed from the tunnel for the remainder of the tests after these photographic data were obtained.

Balance data were then obtained for the various angle of attack and air-injection-rate configurations at a tunnel velocity of 100 fps. Balance tares were also recorded at zero airspeed for the data points corresponding to these configurations. Corresponding balance data were also obtained at 200 fps later in the test period.

Vortex-meter data were obtained by holding the longitudinal (streamwise) and lateral (normal to the chord) positions of the

vortex meter fixed, and surveying the velocities in the vortex in a vertical (spanwise) direction. Surveys were conducted across the vortex from points where zero rotational velocity was noted to exist. At these points, the lateral position was shifted by a fixed increment, and the survey would be repeated. A survey was generally conducted in the lateral direction at a point near the center of the vortex to yield some indication of vortex symmetry, and to check the repeatability of the data. Surveys were conducted at a fixed longitudinal position until all desired data for the various air-injection rates and angles of attack at one longitudinal position were obtained because of the rather lengthy (40-inch) traverse involved between the points at which data were desired. The lateral and vertical increments at which vortex-meter data were obtained varied, as it was desired to obtain at least some data for all configurations within the allocated testing period. Thus, fine grids were mapped for some configurations, while coarse grids were mapped for others. A summary of the configurations for which vortex-meter data were obtained is listed in Table I.

Although vortex-meter data were recorded rather continuously, the wind tunnel was brought down to zero airspeed periodically to allow for the installation of the "calibrator" over the vortex-meter. The tunnel was then again brought up to a speed of 100 fps to check the performance of the vortex-meter.

As had been previously noted, the position of the vortex-meter was monitored by mechanical counters, and its output was monitored by an electronic counter. The reference lateral and vertical positions of the meter and mechanical counters with respect to the model were established by dropping a plumb bob from the longitudinal centerline of the meter to the longitudinal centerline on the tunnel floor, and by direct measurement of

the height of the vortex meter above the tunnel floor. It is estimated that the lateral and vertical positions of the meter were accurate to within ±0.02 inches.

The output of the vortex meter was read out on an electronic counter, which averaged and displayed the rotational speed of the meter for approximately 0.5 second intervals. A further "averaging" was accomplished by mentally recording the digital display of the counter for several periods, and using a median value of the observed readings. For the noninjected configurations, it was sometimes found that several seconds of time would elapse before the observed readings would repeat within a narrow range (say, 3 counts), while for the injected cases, repeatability of readings was noted almost immediately. It is estimated that the rotational velocities obtained from the vortex-meter readings are accurate to within ±3%.

An attempt was made to measure the rotational velocities in the tip vortices by means of hot-wire probes. "X"- array probes, manufactured by the Flow Corporation, which were available at NSRDC, were used during the tests. The probes were mounted such that the active wire was parallel to the airstream when both probes were positioned at the tunnel centerline on the swivel. The hot-wire surveys were conducted after some of the vortex-meter data were taken so that the locations of the tip vortices at 1.5 and 6.5 chordlengths behind the trailing edge of the model were known, and simplified the "search" for the vortex core. The swivel mechanism was cycled through a range of ±15 degrees with respect to the tunnel centerline from a starting position of 15 degrees with respect to the tunnel centerline. The vertical height of the probes was incremented manually, and the surveys were repeated across the area of influence of the vortex. In spite

of the advantage of knowing the position of the tip vortices, quantitative data in terms of the rotational velocities in the tip vortices were not obtained because of a nonlinear output of the hot-wire at low (0-20 fps) rotational velocities which was compounded by an unusual sensitivity of the hot-wire output as regards its orientation with respect to the free stream. Problems were also encountered with a zero drift of the output as the probes were cycled through from their starting positions and returned. These problems could not be resolved during the allocated testing time, and little confidence was held for the limited data which were obtained during the test.

Although two pressure transducers were installed on the model, a short circuit was found to exist in the electrical system of the transducer located at the 50 percent span of the model, apparently in the lead wires which were embedded in the model, and this problem was also not resolved. Data from the outboard transducer showed no variation in its steady component at a fixed angle of attack for any of the air-injection configurations, and these data are commensurate with the balance data, which also indicated only small changes in the forces and moments for the corresponding configurations. The magnitude of the oscillatory component of the pressure, however, generally increased with increasing mass flow through the nozzle as expected. The frequency spectrum of the oscillatory pressure data for the various air-injection configurations was not determined. The pressure data and hot-wire data were the only data which were recorded simultaneously during the tests, since it would have been rather awkward and perhaps, not feasible to record the balance data, vortex-meter data or photographic data concurrently.

In the midst of the test program, the installation of the appurtenances for the generation, illumination and the photographing

of the helium bubble was completed, and approximately two days of testing time were expended in photographing various angle of attack and air-injection rate configurations. The bulk of the photographic data of the helium bubbles was taken at a tunnel airspeed of 50 fps. Consequently, not all of the configurations for which vortex-meter and balance data were obtained at a tunnel velocity of 100 fps were photographed with the helium bubbles, and no photographs of the helium bubbles were taken at a tunnel velocity of 200 fps, although some of these configurations were observed visually.

IV. DISCUSSION OF RESULTS

A. Photographic Study of Tuft-Grid

Flow-visualization studies of the effect of the injection of air into the tip vortex were conducted in part by observing and photographing the changes in the swirl pattern on a tuft grid for various test conditions. The grid was positioned approximately 6-1/2 chordlengths downstream of the trailing edge of the model, and the tunnel velocity for these tests was 100 fps.

Figure 7 shows the swirl pattern on the grid for the non-injected case at a model angle of attack of 10 degrees. Figures 8 through 10 show the swirl pattern for mass injection rates of 0.062, 0.092 and 0.146 lb/sec, respectively, at the same angle of attack. In these photographs, the blurring of the tufts indicates the severity and the extent of rotation in the area influenced by the rotation of the solid core of the vortex. A "reference" tuft of a contrasting color was positioned on the grid at a point which corresponded to that of the tip of the model, so that any displacement of the center of the core of the vortex could also be observed. Figure 8 shows the significant reduction in the swirl pattern on the grid when 0.062 lb/sec of air was injected through the slot. As the mass injection rate was increased to 0.092 lb/sec, the observed swirl velocity was noted to decrease further (Figure 9). Figure 10, showing the tuft grid at a mass injection rate of 0.146 lb/sec, exhibits a remarkable difference from that shown in Figures 8 and 9. The pattern observed on the tuft grid is nearly identical to that observed for a free turbulent jet mixing with a linear stream, i.e., it is seen to be a large area of turbulence which results from the mixing of two flow fields with little noticeable vorticity.

Figure 11 shows the swirl pattern on the tuft grid for the non-injected case at a model angle of attack of 7 degrees, and Figures 12 and 13 show the swirl pattern for mass injection rates of 0.034 and 0.062 lb/sec, respectively at the same angle of attack. The same general comments can be made for the swirl patterns for the 7-degree angle of attack configuration, except that the free-turbulent-jet effect could not be observed at the highest mass flow rate (0.062 lb/sec) considered for this angle of attack. It could be also seen that the swirl distributions of the tufts are not as easily discernible at the lower angle of attack, as the area influenced by the rotation of the core was diminished. Studies of the swirl patterns were also attempted at an angle of attack of 4 degrees with less success as could be expected, and a finer grid would have been required to demonstrate the results of the mass injection noted by other techniques more effectively.

The noted changes in the swirl patterns on the tuft grid were correlated to some extent with the flow at and near the tip of the model by tacking a tuft near the exit of the nozzle. A general diffusion of the swirl pattern as indicated by this tuft could be seen between the injected and non-injected configurations, as well as the inboard displacement of the tip vortex with increasing angle of attack, and the outboard displacement of the tip vortex with mass injection. Rotational velocities of this tuft, as could be made using a strobe, were not measured and the interpretation of the effects of mass injection as noted solely by the changes in the pattern of this tuft would not have been sufficient to determine whether any beneficial changes were being effected by the injection.

B. Photographic Helium-Bubble Study

Figures 14 through 23 show the visualized flow with the model at an angle of attack of 10 degrees and for a free stream velocity of 100 feet per second. These photographs of the illuminated helium bubbles show the concentrated tip vortex core and moderated secondary swirling flow outside the rotation area of the core

of the vortex for no blowing, as well as the effect of mass injection in dissipating the vortex core with blowing. The photographs presented in Figures 14 through 23 are representative illustrations of the various test conditions and results which were obtained in the experiment.

Figure 14 shows a side view of the visualized flow field for the airfoil at an angle of attack of 10 degrees with no blowing, and Figures 15 through 17 show the visualized flow field for moderately increasing amounts of blowing. Figure 14 shows the concentrated tip vortex as well as the moderated swirling outside the core. The photograph shows that the core is formed quite rapidly, within two chordlengths downstream, with a slight increase in the vortex core size as it progresses downstream. Figure 14 also shows that the center of the tip vortex core moved inboard as the vortex progressed downstream. The solid line observed in the photograph is the vortex core and the vortex core diameter is approximately 5 percent of the chord.

Figures 15 and 16 are photographs of the tip region with the wing at a 10° angle of attack for a free-stream velocity of 100 feet per second after moderate amounts of a linearly-directed mass flow had been introduced at the tip of the airfoil. Figure 15 shows the tip vortex with 0.034 lb/sec mass flow injected into the tip vortex core. It can be observed that the tip vortex is no longer as concentrated as before. In addition, the moderated swirl pattern outside the solid core rotation is still clearly observable above the tip vortex core. Figure 16 shows the swirl pattern of the flow field for a mass injection rate of 0.045 lb/sec which was the rate just prior to almost complete dissipation of the vorticity. It can be observed that the concentrated core of the tip vortex has been diffused and only an overall swirl remains. Figure 17 shows the tip region and flow field for 0.062 lb/sec mass flow injected into the tip

vortex core. The photograph shows that there is no well-defined solid core rotation as is discernible in Figure 14, but that there is an overall swirling flow remaining. A comparison of photographs in Figures 16 and 17 apparently shows that the flow characteristics of the injected tip vortex are not changed too much by increasing the mass flow from 0.045 lb/sec to 0.062 lb/sec.

Figures 18 through 20 show top views of the visualized flow field for the airfoil at an angle of attack of 10 degrees with m_i=0, 0.034 lb/sec, and 0.062 lb/sec, respectively. Because of the unusual reflection pattern of the light source on the model, it is convenient to refer to the sketch of the model as viewed from above that is presented on the following page. The bright area of light, trapezoidal in shape, from which the tip vortex emanates, represents a region of reflected light from the model tip. However, this area of light does not represent the entire model tip, as the model tip only appears in the upper left-hand corner of this region of light.

Figure 18 shows the visualized flow field for no blowing and it indicates that the tip vortex core streams off the airfoil in a relatively straight line, and is aligned parallel with the free-stream direction. If the axial coordinate (i.e., z-direction) of the non-injected tip vortex core were extrapolated linearly to the airfoil, it would be found to emanate approximately from the 75 percent chord. It can be also noted from Figure 18 that there is an upward-curling of the air flow around the model tip. This upward-curling flow eventually spirals into the tip vortex core.

Figure 19 presents the visualized flow field for 0.034 lb/sec of injected mass flow. The photograph shows that injection of an airstream into the core of tip vortex is beginning to diffuse the tip vortex. It can be noted that the same general upward-curling of the air flow around the model tip can be seen in Figure 19 when the blowing is on. This may suggest that

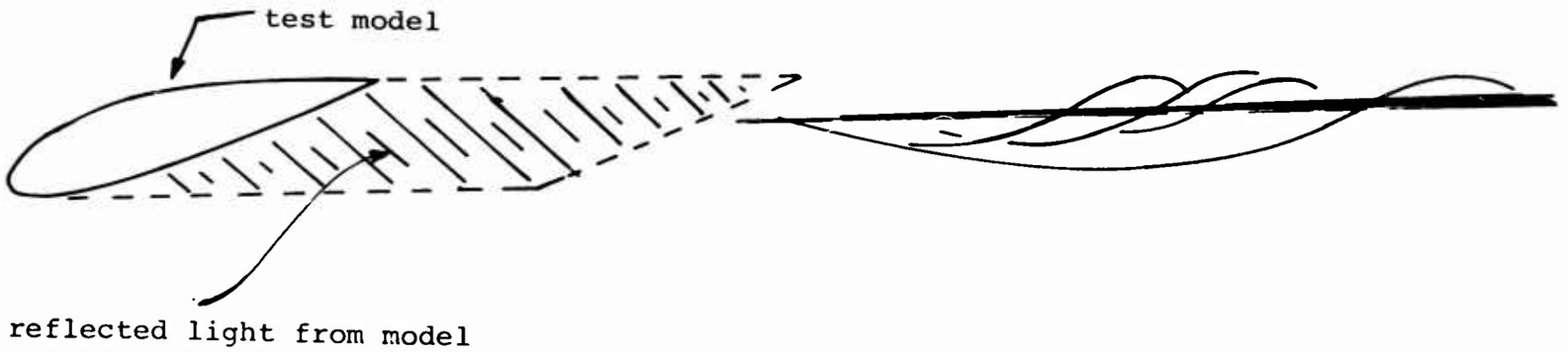

TOP VIEW OF TEST MODEL SHOWING
AREA OF REFLECTED LIGHT

the injected flow does not significantly interact with the wing flow at the wing tip. If the axial coordinate (z-direction) of the injected tip vortex core was extrapolated linearly to the airfoil, it would be found to emanate approximately from the 25 percent chord.

Figure 20 presents the flow pattern for a mass flow injection of 0.062 lb/sec. This photograph shows that the vortex core has been considerably diffused by injecting the airstream. It can be noted that the upward-curling flow around the model tip does not appear to be significantly affected with increased blowing.

Figure 21 presents the visualized flow field for no mass injection at 12 chordlengths downstream. The photograph shows the concentrated core of vorticity which increases slightly as it progressed downstream.

An interesting feature observed in Figure 21 is that it shows helium bubbles from the free stream feeding into the area surrounding the tip vortex core as the tip vortex core progressed downstream. Thus, the tip vortex attracts fluid particles from the free stream either into its core or within the moderate swirl area surrounding the tip vortex core at downstream locations. It is believed that the solid line observed in the photograph represents the tip vortex core, but this is open to interpretation as to what one wishes to define as the vortex core for an actual three-dimensional helical vortex flow field.

Figures 22 and 23 show the visualized flow field for injected mass flows of 0.034 lb/sec and 0.062 lb/sec, respectively, at a downstream location of twelve chordlengths. Figure 22 still shows a concentrated core of vorticity for an injected mass flow of 0.034 lb/sec although, perhaps, a slight increase in vortex size may be noted. Figure 23 as compared to Figure 22

shows that the concentrated core of vorticity has been diffused and dissipated with only a moderated swirling flow remaining at a mass injection rate of 0.062 lb/sec. This photograph shows that, at least, the concentrated tip vortex core was noticeably diffused by injection of an airstream. While no pictures could be taken, visual inspection of the remaining swirling flow field in the diffuser down to the turning vanes indicated that the remaining swirling flows never reformed into the kind of a concentrated core of vorticity depicted in Figure 14 for a non-injected tip vortex core.

C. Vortex-Meter Measurements

While the flow-visualization studies conducted illustrate certain significant effects qualitatively, it is believed the important characteristic of the injected flow field is the vorticity associated with the tip vortex core. The concentration of vorticity into a relatively small core determines the magnitude of the pressure changes occurring on a following rotor blade of a helicopter or on fixed-wing aircraft following in the wake of the generating aircraft.

D. Evaluation of Vorticity from Test Data (Contour Plots)

Contour plots of the vorticity and plots of the maximum vorticity distribution through the tip vortex core that were made behind the wing for $\alpha=10°$ and for various blowing values are presented in Figures 24 through 29 for a free-stream velocity of 200 feet per second. It should be noted that the center of origin depicted in the contour plots are relative to the center of the vortex at 1-1/2 and 6-1/2 chordlengths downstream and do not show the absolute shift which occurred in the center of the vortex as it progressed downstream. Thus, the dimensions in the y and z-directions are relative to the center of the vortex core. In general, it was found that the effect of blowing was to move the vortex core inboard at 1-1/2 chordlengths and outboard at 6-1/2 chordlengths downstream.

The spanwise surveys that are presented in Figures 26, 29, 30 and 31 are those for which the maximum vorticity was measured in a plane perpendicular to the wing chord and parallel to the span. The lines of constant vorticity presented in the contour plots presented in Figures 24, 25, 27 and 28 are the actual counts in rev/sec as recorded by the vortex meter.

Figure 24 compares the contour maps (i.e., vorticity) for zero blowing for a model angle of attack of 10° at 1-1/2 chordlengths and 6-1/2 chordlengths behind the wing. It can be seen that the vortex remains relatively fixed in size as it progresses downstream. It may be noted that a maximum of 960 counts per second was measured by the vortex meter at 1-1/2 chordlengths as compared with 650 counts per second at 6-1/2 chordlengths as a result of the redistribution of vorticity through the action of viscosity. However, the vortex strength of the non-injected tip vortex remains almost constant as a result of the continual wrapping up of a vortex sheet. The measurable rotating fluid extends over a circular region of approximately 1.6 inches in diameter (the contour plots are drawn to a 2.5:1 scale).

Figure 25 compares the contour maps of vorticity distribution at 1-1/2 and 6-1/2 chordlengths at a mass flow rate of 0.062 lb/sec for a free stream velocity of 200 feet per second with the model at a 10° angle of attack. Comparison of Figure 25 with Figure 24 indicates that the maximum vorticity 1-1/2 chordlengths behind the wing has been changed more than it has at 6-1/2 chordlengths. For instance, the maximum count at 1-1/2 chordlengths has been reduced from 900 to 700 cps while at 6-1/2 chordlengths the count was reduced only from 650 to 580 cps.

It may be noted that the outboard area of the contour plot in Figure 25 for 1-1/2 chordlengths downstream is distorted. It is believed that this may be due to the influence of the injected mass flow from the nozzle at the wing tip. The velocity distribution of the nozzle was "triangular" rather than uniform and thus the injected mass flow may impart a swirl component

to the fluid as it leaves the nozzle. Also, near the inboard edge of the slot, reversed flow occurred.

The contour map depicted on the right-hand side in Figure 25 gives the vorticity distribution at 6-1/2 chordlengths for an injected mass flow rate of 0.062 lb/sec. As a result of diffusion of the tip vortex core, the distorted area noted at 1-1/2 chordlengths has been "smoothed out" and the vortex has a more circular appearance. A comparison of the contour maps between 1-1/2 and 6-1/2 chordlengths shows that the injected mass is beginning to have a significant effect on the vorticity distribution as the contours representing constant rotational speed are being decreased in magnitude from 1-1/2 chordlengths to 6-1/2 chordlengths and are spreading outward as the vortex core progresses downstream.

A plot of the vorticity distribution of the tip vortex core in the YZ-plane is presented in Figure 26 with the wing at a ten degree angle of attack for a free stream velocity of 200 feet per second. The plot shows the maximum vorticity which was measured in a plane perpendicular to the wing and parallel to the span. The Z-dimension is along the span of the wing with the numbers increasing from the wing root.

Figure 26 compares the vorticity distribution for zero blowing and with those obtained for a mass flow rate of 0.062 lb/sec. The maximum vorticity at 1-1/2 chordlengths behind the wing has been changed more than it has at 6-1/2 chordlengths as shown by the decrease in the vorticity distribution. The plots also indicate that the effect of mass injection has moved the center of the vortex inward at 1-1/2 chordlengths and outward at 6-1/2 chordlengths.

Figure 27 compares the contour plots at 1-1/2 and 6-1/2 chordlengths for an injected mass flow rate of 0.091 lb/sec. Again, the tip vortex core appears distorted at 1-1/2 chordlengths while the action of viscosity smooths the contours at 6-1/2

chordlengths. As depicted in Figure 27, the injected mass has had a significant effect on the vorticity associated with the tip vortex core. Compared with the contour map at 6-1/2 chordlengths for m_i=0.062 lb/sec. Figure 27 shows that the magnitude of the contours representing constant rotational speed have reduced by a factor of approximately one-half. The significant reduction in the magnitude of the contours representing constant rotational speed supports the conclusion that an important change took place in the vorticity distribution as the mass flow was increased from 0.062 lb/sec to 0.091 lb/sec.

Figure 28 presents contour plots of constant vorticity for the highest blowing coefficient used (0.146 lb/sec injected mass flow). It can be seen that while there is some peaking-type vorticity distributed at 1-1/2 chordlengths, there is none at 6-1/2 chordlengths. At 6-1/2 chordlengths, Figure 29 shows there is no well-defined core, and indicates only a small measurable rotational component in the fluid. During the test no reforming of the tip vortex was observed to have occurred downstream and thus the strength associated with the non-injected core was effectively dissipated within 6-1/2 chordlenths by linear mass injection.

A plot of the vorticity distribution that was made behind the wing for α=10° for a free-stream velocity of 200 feet per second is depicted in Figure 29 for the highest mass injection rate used, 0.146 lb/sec. While there is still a peaking-type of vorticity distribution at 1-1/2 chordlengths, there is no observable peak at 6-1/2 chordlengths. Also, the characteristics of the vorticity distribution at 6-1/2 chordlengths have been changed completely. The magnitude of the measurable vorticity has been significantly decreased. The flow pattern at this mass injection rate resembled that of a free-turbulent jet.

Plots of the basic vorticity distributions that were made behind the wing for α=10° for a free-stream velocity of 100 feet per second are presented in Figures 30 and 31.

Figure 30 compares the vorticity distribution for zero blowing with the distribution obtained for the lowest mass injection coefficient at 1-1/2 chordlengths and 6-1/2 chordlengths for the 100 feet per second case. The plots indicate that while the vortex center remained relatively fixed at 1-1/2 chordlengths, the effect of mass injection at 6-1/2 chordlengths again moved the center of the vortex outward at 6-1/2 chordlengths.

Figure 31 presents survey plots for a mass injection rate of 0.091 lb/sec. This plot is very similar to the results presented for the 200 feet per second case with a mass injection rate of 0.146 lb/sec. At 6-1/2 chordlengths, the mass injection of the tip vortex core has resulted in a significant dissipation of the vorticity associated with the tip vortex core.

As a result of the distortions occurring in the contour plots of constant vorticity as depicted in Figures 25 and 27 the tip vortex core was by no means circular in appearance and it was necessary to use a 3-dimensional numerical integration technique in conjunction with a curve-fitting procedure to obtain the vortex strength (i.e., integrated vorticity) associated with the tip vortex core. The curves for the integrated vorticity presented in Figure 32 were determined from the resultant contour plots by employing the numerical integration technique.

Figure 32 shows the change in the measured integrated vorticity associated with the injected tip vortex core at 6-1/2 chordlengths behind the airfoil for various amounts of mass flow injection at free-stream velocities of 200 feet per second, and for model angles of attack of 10° and 7°. Both curves presented indicate that blowing can significantly reduce the strength of an injected vortex. The curves show that there is a slight initial decrease in vortex strength when a small amount of mass is injected into the tip vortex core. The vortex strength then decreases rather quickly with increasing mass flow for both cases.

The reason for a distinct region of rapid dissipation in downstream vorticity with increased blowing as observed in Figure 32. is not, as yet, fully understood. While a significant decrease in vortex strength may be expected on the basis of theory (Ref. 4), the magnitude of the decrease is somewhat surprising. It may be that a rapid dissipation and diffusion of the vorticity associated with the injected vortex core could result from a "kink" instability or vortex breakdown created in the tip vortex core by the turbulent jet. This would occur at different blowing rates for the 10° and 7° angle of attack cases as the results show due to the fact that a larger mass flow would be required to modify the stronger tip vortex core which occurs at the higher (10°) angle of attack as a result of the greater lift which is developed. Once precipitated, the instability would change the scale of turbulence in the vortex core perhaps leading to a greater dissipation of the concentrated vorticity than if an instability had not been generated. If the instability does occur then simply increasing the mass flow into the core would probably not be important in changing the flow characteristics of the injected vortex.

The following brief argument is given to show why a vortex breakdown may have occurred in these tests. According to Bossel (Ref. 5) vortex breakdown is the rapid expansion over a short axial distance (of the order of the thickness of the rotational core) of stream tubes centered about the axis of a rotationally symmetric vortex. The breakdown may or may not result in stagnation on the axis and reversed flow, and it may or may not be accompanied by breakdown into turbulent flow. The flow field may be incompressible or compressible, inviscid or viscous. In some cases (supersonic vortex breakdown, for example), it is not clear whether a stagnation point and reversed flow exist. In most other cases, stagnation points on the axis and axial-flow reversal have been observed. From the results of experiments by various investigators, the following conclusions have been drawn:

(1) The primary variable is swirl. Breakdown will not occur at low swirl values.

(2) The axial pressure gradient affects the breakdown position. An adverse pressure gradient can, apparently, precipitate a breakdown which would not otherwise occur.

(3) Mach-number effects are minor.

(4) Influence of upstream turbulence is small, but influence of downstream disturbances is pronounced.

Bossel introduced a stability criterion based upon a simplified model. By considering nearly solid-body rotation close to the axis, and assuming that the vortex has constant axial velocity (v_z) over the vortex-core radius, $0<r<r_c$, Bossel showed that the swirl angle (ϕ_c) taken at $r=r_c$ is of critical importance to the behavior of the vortex flow. The swirl angle is defined by

$$\phi_c = \arctan \frac{(v_\theta)_c}{(v_z)_c} = \arctan \left(\frac{\text{swirl velocity}}{\text{axial velocity}} \right)_{\text{at } r=r_c} \qquad (1)$$

It has been noted that all observations of breakdown have maximum swirl angles of approximately 54° (i.e., $v_\theta \simeq 1.4\ v_z$). This also agrees with theoretical values given by Squire (1960) and Hummel (1965).

Considering the curve for the circulation (at 6.5 chord-lengths) for the wing at 7° angle of attack for a free stream velocity of 200 feet per second, it may be noted that the circulation has a value of about 4.5 ft^2/sec at a mass injection rate of 0.062 lb/sec just after the rather significant decrease in the circulation curve. By using this value of the circulation, it is possible to estimate the values of the swirl and axial velocities using previously developed expressions (Ref. 4). For no mass

injection, it was discovered that the swirl angle defined by Bossel had the following order of magnitude:

(a) mass flow = 0.0 lb/sec

v_θ = swirl velocity = 90 fps (order of 1/2 free stream)

v_z = axial velocity = 200 fps (order of free stream)

and from Bossel's criteria we find that the swirl angle is given by

$$\phi_c = \arctan\left(\frac{90}{200}\right) \sim 22°$$

which is much less than the 54° at which vortex breakdown occurs. However, for the injected vortex core,

(b) mass flow = 0.062 lb/sec

and from Bossel's criteria we find that the swirl angle is given by

$$\phi_c = 51°$$

which suggests that vortex breakdown may be expected to occur in a range near this mass flow rate.

The following listing gives estimates of the swirl angle for the various test conditions noted:

angle of attack α	free stream velocity V	swirl angle ϕ_c	mass injection m_i
7°	100 fps	49°	.034 lb/sec
10°	100 fps	48°	.045 lb/sec
7°	200 fps	51°	.062 lb/sec
10°	200 fps	50°	.091 lb/sec

For the cases depicted, it can be seen that the swirl angle is approaching a value close to 54° at mass flow rates where it was observed visually that the tip vortex core was being significantly dissipated. This suggests the presence of a vortex-breakdown phenomena.

Physically, linear injection of a tip vortex core will cause a change in axial pressure gradient and decay of the swirling motion as a result of the viscous mixing of the two flow fields. The effect of the decay of the swirling motion is to further increase the pressure in the vortex core and, consequently, to decrease the axial velocity there. If the axial-velocity retardation (i.e., axial velocity defect) is sufficient such that the swirl angle approaches 54°, then the vortex-breakdown phenomena can occur.

Regardless of the mechanism, experimental results indicate that the concentrated vorticity associated with a trailing tip vortex can be significantly dissipated (i.e., dissipation greater than 80 percent for the highest blowing rates considered) by injection of an airstream into the forming tip vortex core. While it cannot be demonstrated from the data presented, it is believed that due to the significant turbulence created in the vortex within 6-1/2 chordlengths downstream resulting from the injection technique, the vorticity remaining at that location would be quickly dissipated further downstream.

Figure 33 presents a comparison of measured and theoretical results of circulation strength versus mass flow rates for a free stream velocity of 200 feet per second for both a 10° and 7° model angle of attack.

From Figure 33 it can be observed that the theoretical curve for a 10° model angle of attack follows the trend of the experimental curve in the lower mass flow range until an injected mass flow rate of about 0.062 lb/sec is reached. Beyond this point, the theoretical curve decreases slightly while the

experimental curve continues to decrease significantly with increasing blowing showing that it is possible to significantly dissipate the vortex core by mass injection. Generally speaking, the assumptions employed in the theory were applicable for flow fields that change slowly in the stream direction. The experimental results show that at the higher mass injection rates significant changes have taken place in the vortex core structure in both the tangential and streamwise directions within the near flow field (i.e., within 1-1/2 chordlengths) where the theory was not applicable but did predict qualitatively what could be expected from mass injection. It is seen that Figure 29 illustrates that clear and significant advantages can be obtained by linear mass injection of the trailing tip vortex core.

The theoretical curve at 6-1/2 chordlengths downstream for a 7° model angle of attack follows the same trend as the 10° case. Correlation between a theory based upon the Reynolds stresses of the injected flow field and experimental results were obtained in the lower mass flow range. Again, the possibility is not ruled out that the jet may have created an instability in the tip vortex core causing a significant change in the turbulent eddy viscosity at the higher injected mass flow rates. The significant decrease of measurable vorticity observable in the experimental results with increasing blowing demonstrates that it is possible to significantly dissipate the trailing tip vortex by mass injection.

Note that the theoretical curves in Figure 33 for lower mass injection rates predict a greater change in vortex strength than was actually attained in the experiment. This implies that the most efficient use of the injected mass flow was not yet obtained. It is believed it should be possible with judicious design changes to obtain an even more efficient use of the injected mass than indicated in these experimental results.

Balance Data Measurements

Effects of the jet-induced vortex dissipation on basic performance parameters are shown in Figures 34 through 37 for a free-stream velocity of 100 feet per second, and in Figures 38 through 41 for a free-stream velocity of 200 feet per second. It can be observed in Figure 34 and Figure 38 that the lift force at a fixed angle of attack remained almost constant for either a free-stream velocity of 100 feet per second or 200 feet per second with increasing mass injection of the tip vortex core. (Note that the geometric angle of attack was not the angle of attack for zero lift.) The rolling moments shown in Figure 35 and Figure 39 also remained constant which indicates that the lift distribution on the wing was not altered by addition of mass flow injection.

Figure 36 shows the effect of mass flow injection on the net drag of the wing for a free-stream velocity of 100 fps. Figure 40 presents the effects of mass flow injection on the total drag and the net drag of the wing for a free-stream velocity of 200 feet per second. The results plotted in Figure 36 shows some increase in net drag with increased blowing for the 100 feet per second case. However, no increase is noted in net drag for the 200 feet per second case where the measured drag forces were 4 times higher than the corresponding values for the 100 feet per second case. Balance data obtained was accurate to within ±.1 lb.

Thus, it is believed that the increases occurring in the measured net drag forced for the 100 fps case are a result of variations in the balance system at very low force measurements. Since the upward-curling flow about the model tip was not affected by chordwise blowing, it is believed that the jet flow did not interact significantly with the wing flow and thus the change in the total drag force as depicted in the top graph of Figure 40 was purely that obtained by "jet thrust." The fact that this drag reduction was obtained with blowing is important as it allows the recovery of the power that must be used to inject the tip vortex core.

The effect of linear mass injection on the pitching moment are shown in Figures 37 and 41 for free-stream velocities of 100 feet per second and 200 feet per second, respectively. Since the balance system accuracy for pitching moment was ±0.15 ft-lb it is believed that the variation of pitching moment versus mass flow presented in Figure 37 for a free-stream velocity of 100 ft/sec has no real meaning. The variation obtained at 200 ft/sec. Figure 41, however, has somewhat of a consistent trend to it even though the balance system accuracy is marginal and thus consideration of this possible destabilizing moment should be given in any future investiation.

V. CONCLUSIONS AND RECOMMENDATIONS

The following conclusions were drawn from the results of the experimental test program and on the basis of theoretical predictions:

- Beneficial effects can be obtained from modification of a tip vortex by chordwise injection of an airstream into the trailing tip vortex core.

- It was found possible to significantly dissipate the concentrated vorticity associated with a tip vortex core under sufficient but moderate mass flow rates at 6-1/2 chordlengths downstream.

- Appreciable reduction of the swirl component of velocity (over 80% reduction at the highest blowing rate considered) of the tip vortex was obtained by axial mass injection in agreement with reductions obtained in the concentrated vortex strength.

- Both the amount of mass injected and velocity at which it is injected are important in modifying the tip vortex cove. However, the relative importantce of these parameters was not delineated in the experiment.

- Flow-visualization studies show that the vortex sheet rolls up quickly (i.e., within one chordlength at 100 fps free stream velocity) behind the airfoil to form a very concentrated core of vorticity. It was observed that a solid non-injected vortex core persists as the vortex progressed downstream.

- Flow-visualization studies show that not only does the vortex sheet wrap up into a non-injected vortex core, but also that fluid particles from the free stream feed into the tip vortex core at locations far downstream (greater than 12 chordlengths).

- Balance data measurements show that it is possible to modify the trailing tip vortices without adverse effects on aircraft performance. Both the mean lift and net drag of the airfoil remained relatively constant over the entire mass flow range. This favorable result occurs because the injection technique does not significantly change the chordwise and spanwise pressure distributions adversely over the airfoil.

- Significant dissipation of the tip vortex core was obtained at several different free-stream velocities (i.e., 50, 100, and 200 feet per second) suggesting that it may be possible to modify the tip vortex core beneficially over a wide flight regime of an aircraft. Although, a fully turbulent flow was developed by means of mass injection, it has not been established by the experiment that the beneficial results obtained could be significantly changed by a Reynolds number effect at the higher free stream velocities.

- It was observed visually and experimentally measured that the effect of blowing on the location of the tip vortex core was to move the center of the tip vortex core inboard in the spanwise direction at 1-1/2 chordlengths downstream and outboard in the spanwise direction at 6-1/2 chordlengths downstream.

It is recommended that:

- A basic research program be conducted to study the initial mixing of a linear and swirling flow in an aerodynamic medium since the present experimental results indicate that the same beneficial results are not obtained at all flight conditions. It is believed important to determine the characteristics of the flow mixing so that the noted beneficial effects can be realized at all flight conditions. The experimental investigation would also determine if an instability is created in the trailing tip vortex core by linear mass injection. Bossel's or Squires's stability criteria would be a good starting point.

- An attempt should be made to determine experimentally what adverse compressibility effects could be encountered in linear mass injection of a tip vortex core at higher wind tunnel velocities than have previously been obtained. Such an investigation should consider the effect of sweep angles on the mass injection technique.

- Serious consideration be given to analytical and experimental studies of the hydrodynamic applications of injecting tip vortices shed by a ship's propellers. In particular, it may be possible to change noise signatures of submarines. Other possible benefits may be the alleviation of tip-cavitation problems in high-speed propeller operation via a mass injection technique.

VI. REFERENCES

1. Spencer, R.H., Sternfeld, H., and McCormick, B.W., "Tip Vortex Core Thickening for Application to Helicopter Rotor Noise Reduction," TR66-1, September 1966, USAAVLABS.

2. Tanner, W,H., and Wohlfeld, R.M., Vortex Field, Tip Vortex and Shock Formation on a Model Propeller, Bell Helicopter Company, Paper presented at Third CAL/AVLABS Symposium, Aerodynamics of Rotary Wing and V/STOL Aircraft, Vol. I, June 1969.

3. Rinehart, S.R., "Study of Modification of Rotor Tip Vortex by Aerodynamic Means," RASA Report No. 70-02, ONR Contract No. N00014-69-C-0169, AD-704804, 1970.

4. Hale, R.W., Tan, P., and Ordway, D.E., "Experimental Investigation of Several Neutrally-Buoyant Bubble Generators for Aerodynamic Flow Visualization," Sage Action, Inc. Report No. RR6901, ONR Contract No. N00014-68-C-0434, AD 717 390, 1969.

5. Bossel, H.K., "Inviscid and Viscous Models of the Vortex Breakdown Phenomenon", Aeronautical Sciences Division Ph.D. Thesis, University of California Report No. AS-67-14, August 1967.

APPENDIX A

SUMMARY OF FIGURES

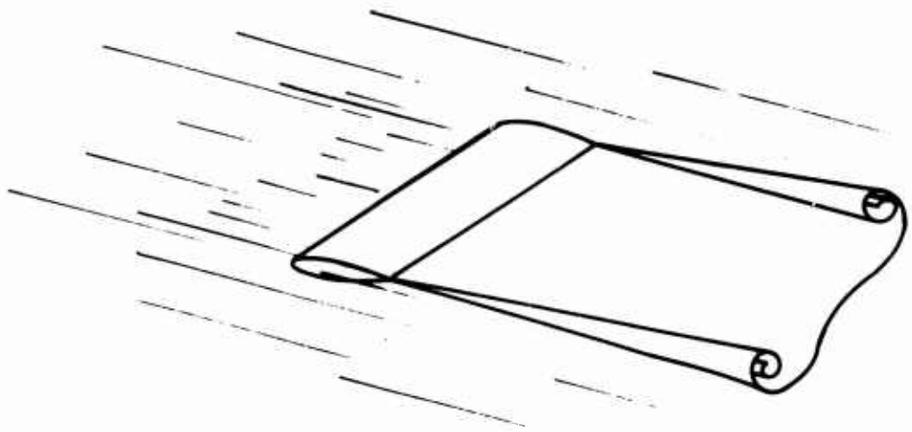

Figure 1. Prandtl's Sketch of the Rolling-Up of a Trailing Vortex Sheet

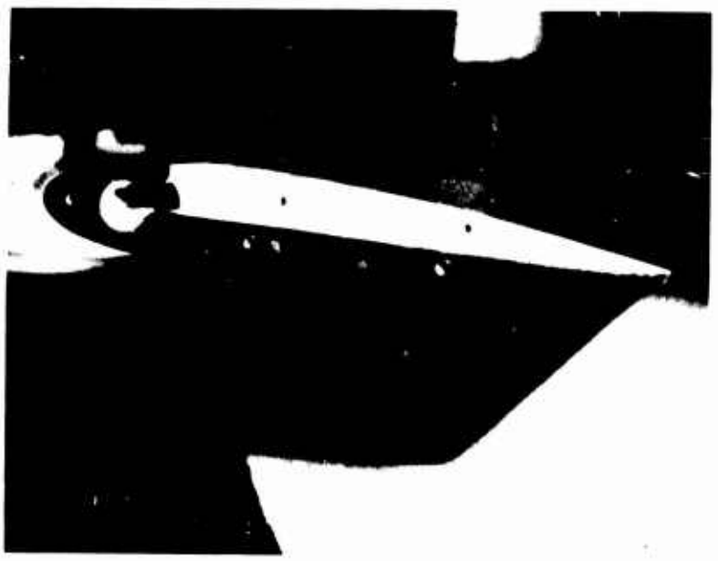

Figure 2. End View of Air-Injection Slot; End Cap Removed

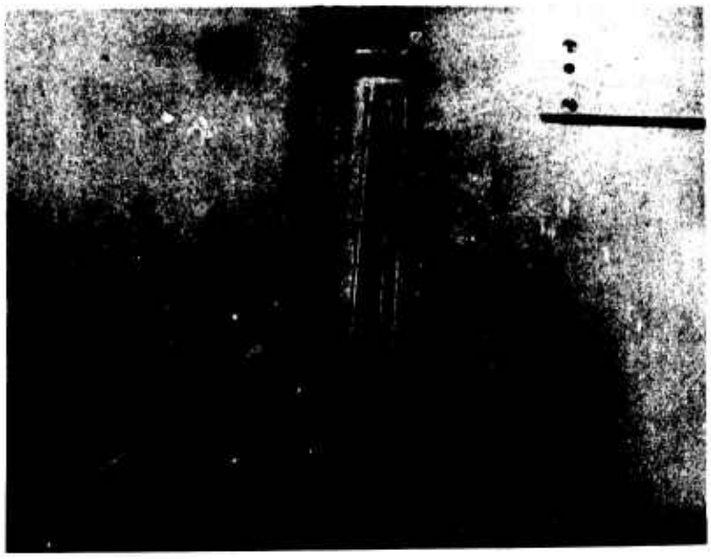

Figure 3. Top View of Air-Injection Slot With End Cap in Place

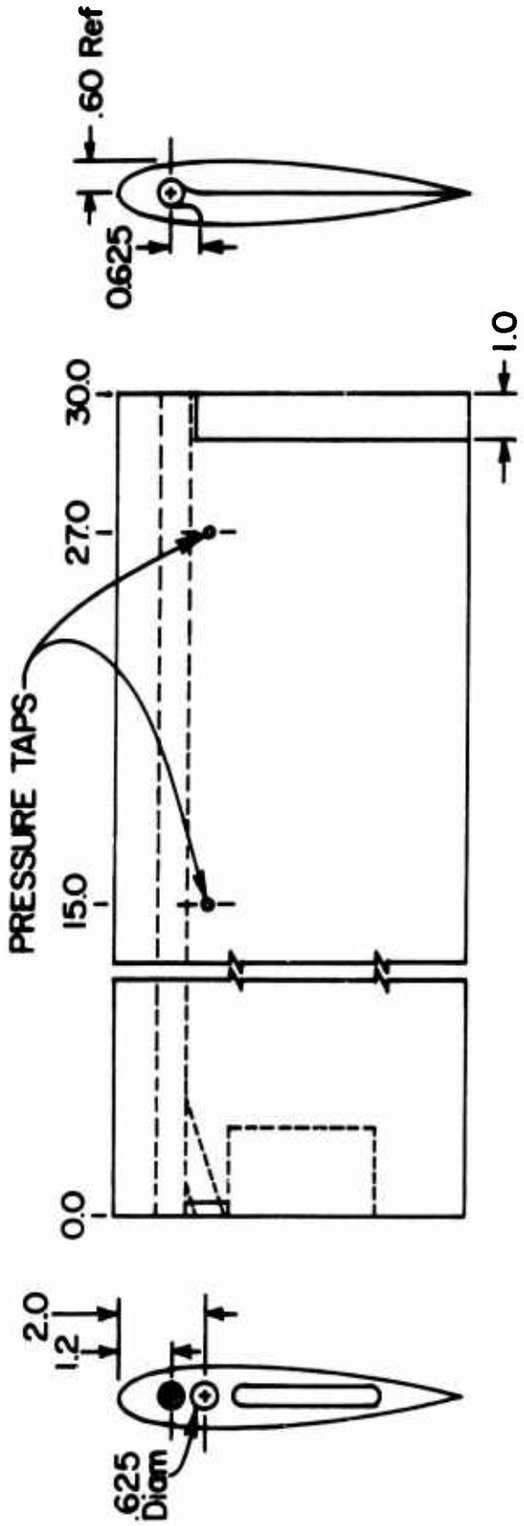

Figure 4. Schematic View of Model

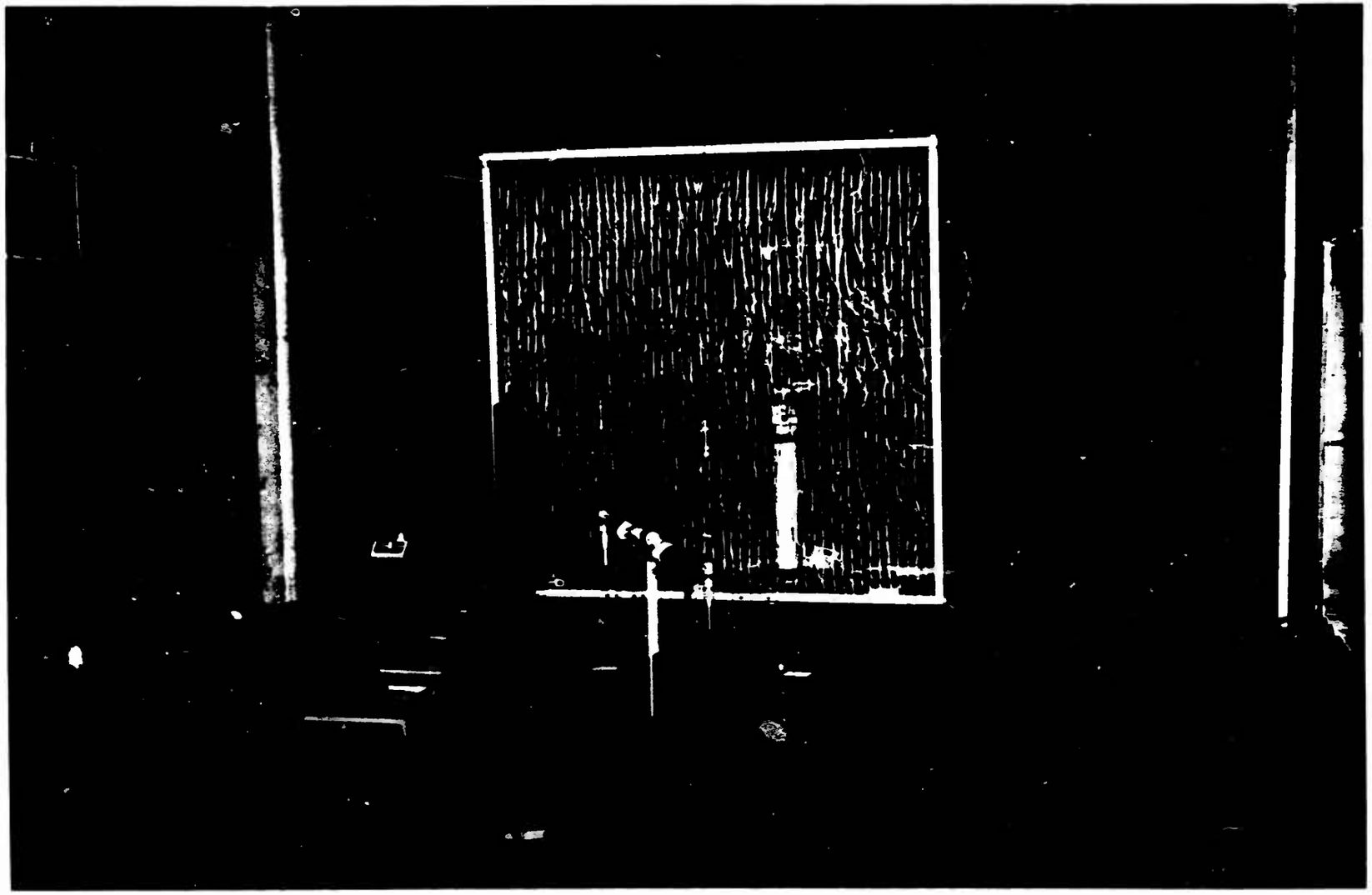

Figure 5. Wind Tunnel Installation of Model and Instrumentation

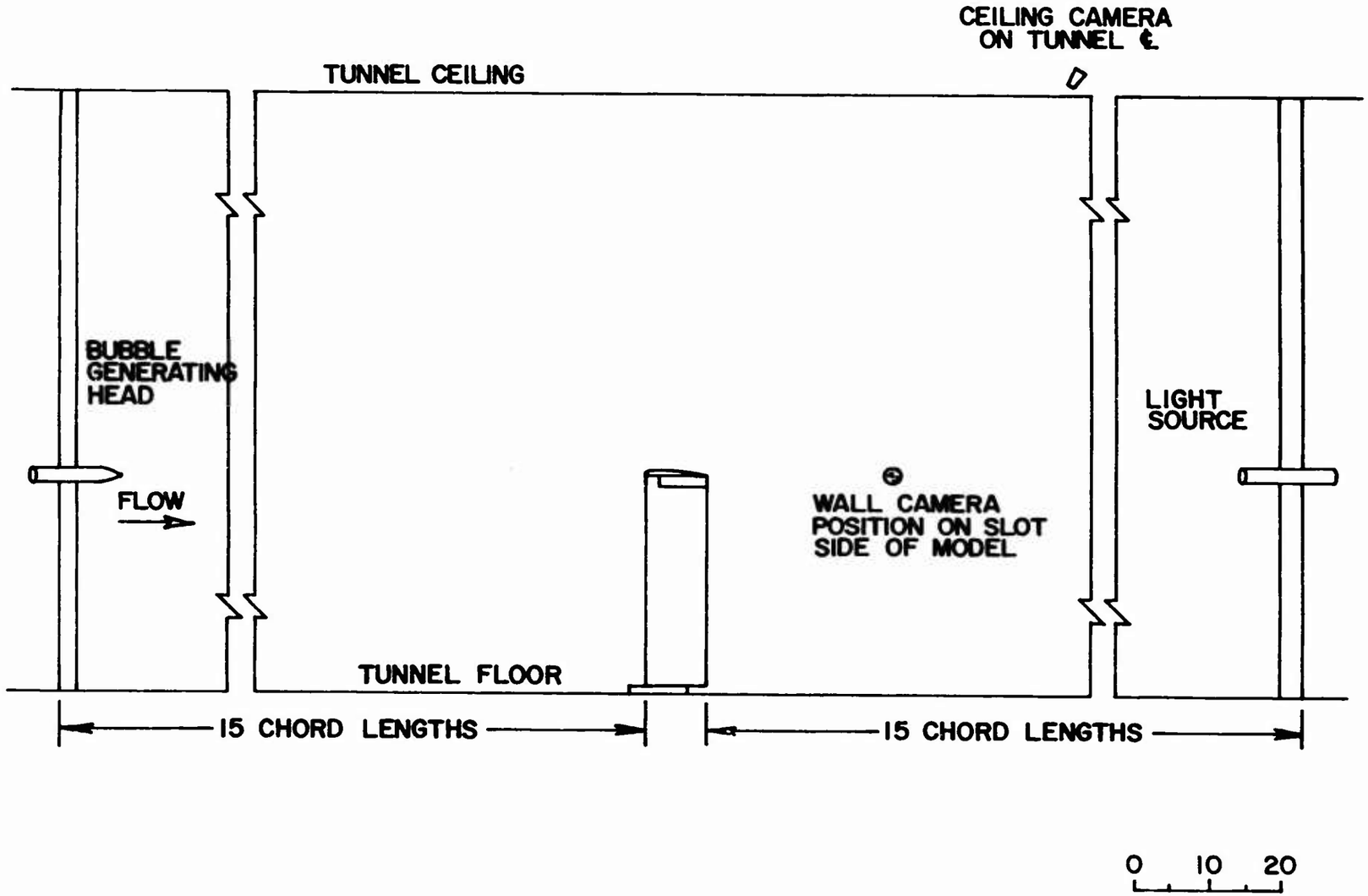

Figure 6. Schematic View of Set-Up for Photographing Helium Bubbles

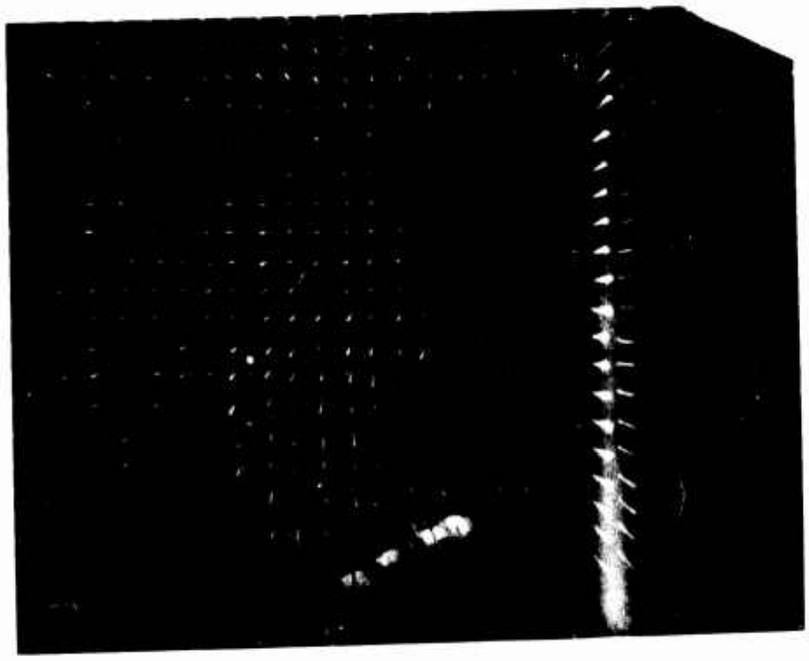

Figure 7. Tuft-Grid Study at 7 Chordlengths Downstream, m_i=0.0 lb/sec, α=10°, V=100 fps

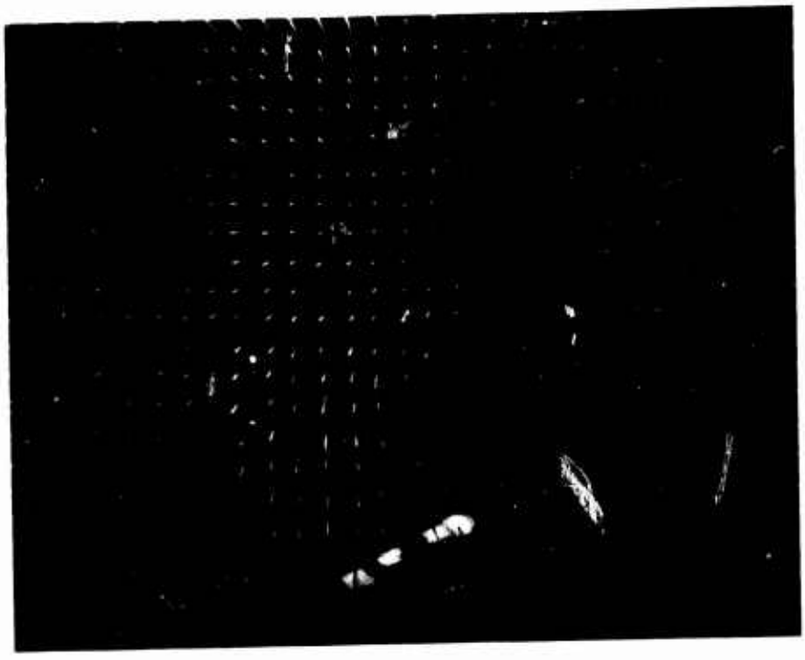

Figure 8. Tuft-Grid Study at 7 Chordlengths Downstream, m_i=.062 lb/sec, α=10°, V=100 fps

Figure 9. Tuft-Grid Study at 7 Chordlengths Downstream, m_i=.091 lb/sec, α=10°, V=100 fps

Figure 10. Tuft-Grid Study at 7 Chordlengths Downstream, m_i=.146 lb/sec, α=10°, V=100 fps

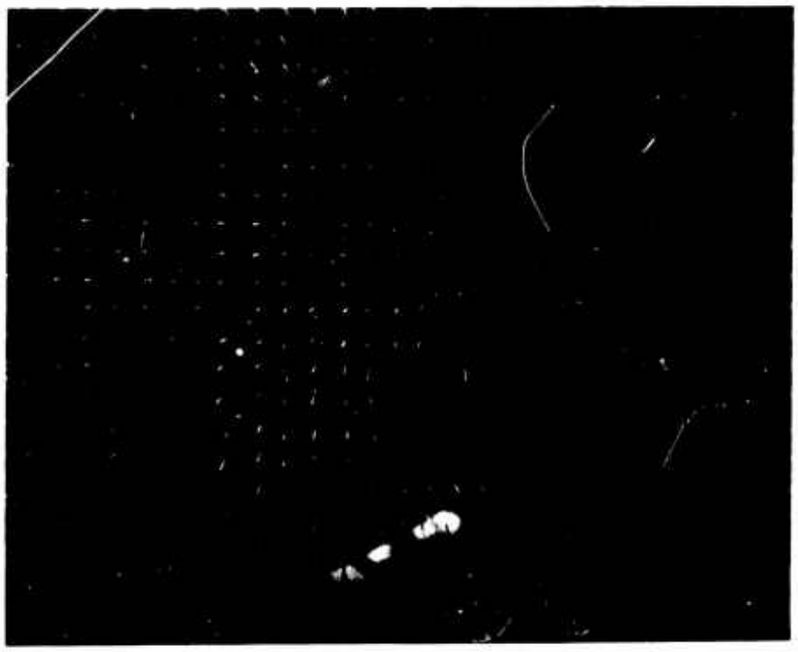

Figure 11. Tuft-Grid Study at 7 Chordlengths Downstream, m_i=0.0 lb/sec, α=7°, V=100 fps

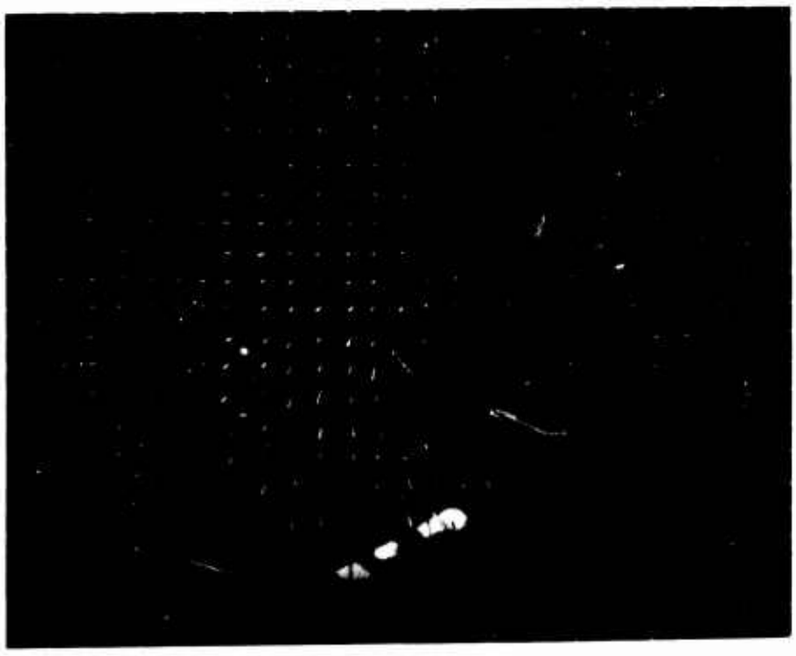

Figure 12. Tuft-Grid Study at 7 Chordlengths Downstream, m_i=.034 lb/sec, α=7°, V=100 fps

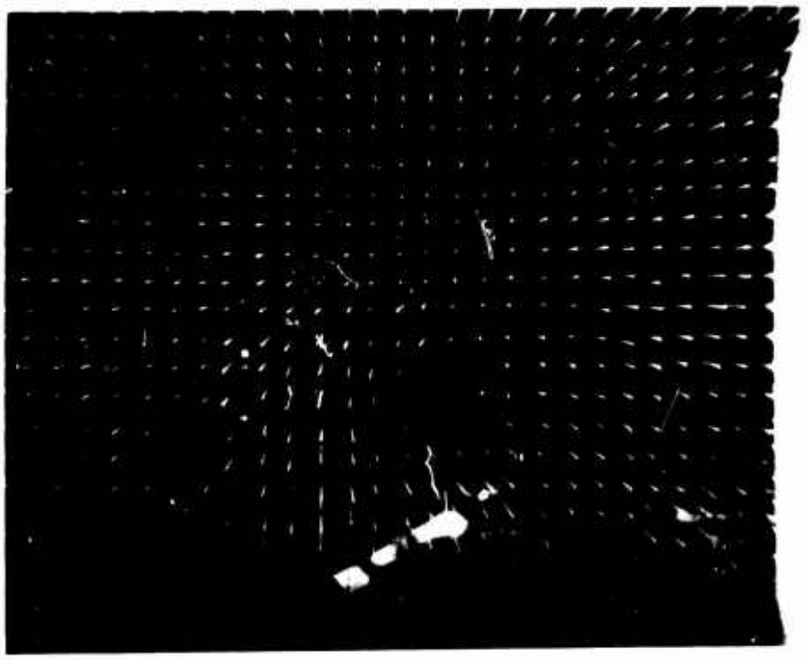

Figure 13. Tuft-Grid Study at 7 Chordlengths Downstream, m_i=.062 lb/sec, α=7°, V=100 fps

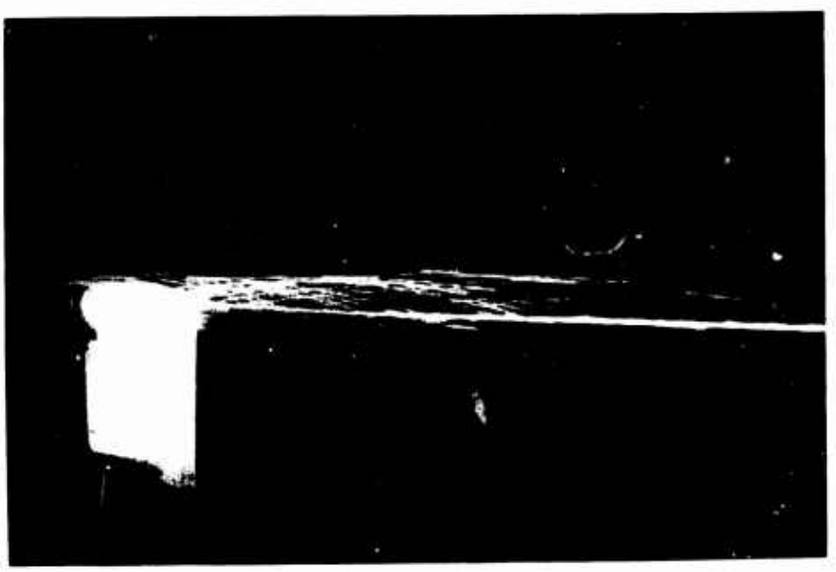

Figure 14. Tip-Vortex Flow Visualization from Side View as Shown by Helium-Bubble Technique for m_i=0, α=10°, and V=100 fps

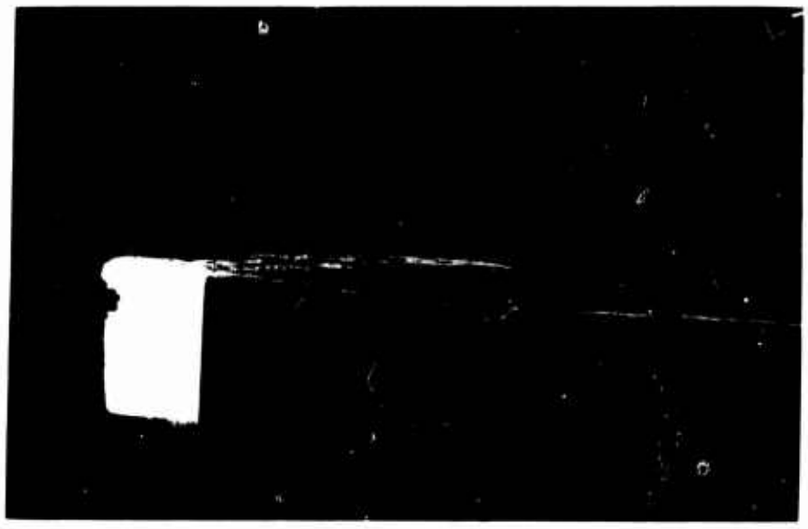

Figure 15. Tip-Vortex Flow Visualization from Side View as Shown by Helium-Bubble Technique for m_i=0.034 lb/sec, α=10°, and V=100 fps

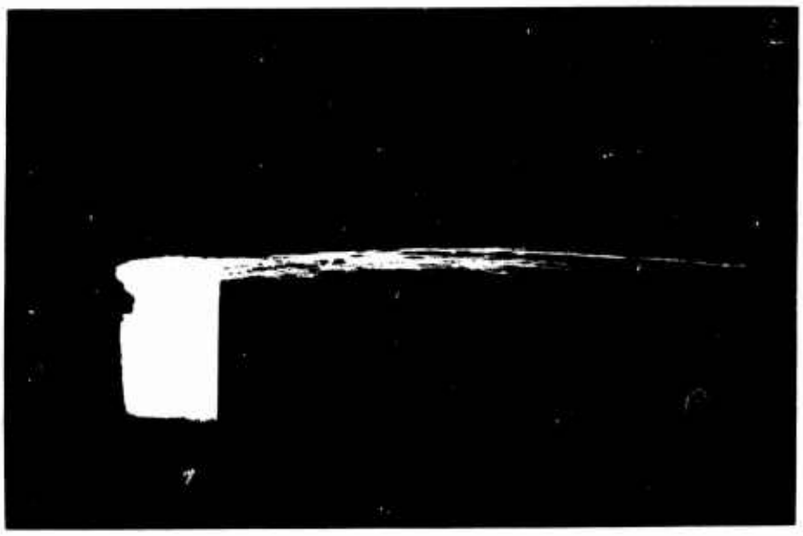

Figure 16. Tip-Vortex Flow Visualization from Side View as Shown by Helium-Bubble Technique for m_i=0.045 lb/sec, α=10°, and V=100 fps

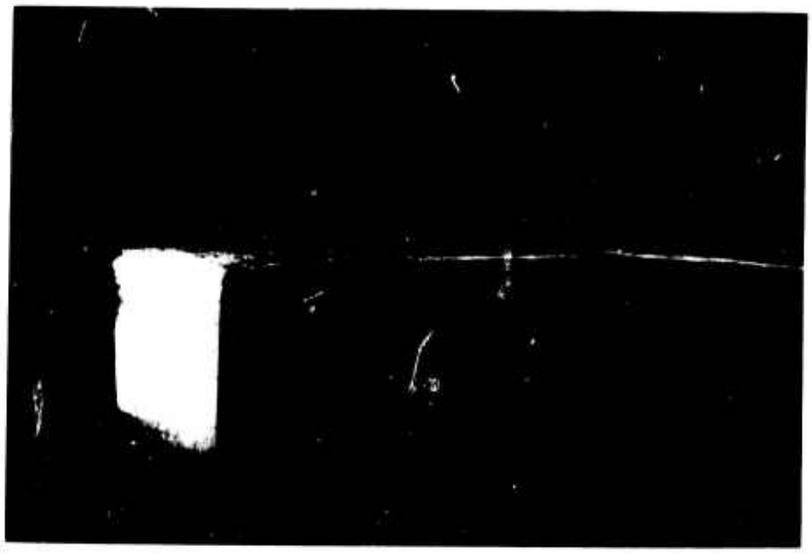

Figure 17. Flow-Field Visualization from Side View as Shown by Helium-Bubble Technique for m_i=0.062 lb/sec, α=10°, and V=100 fps

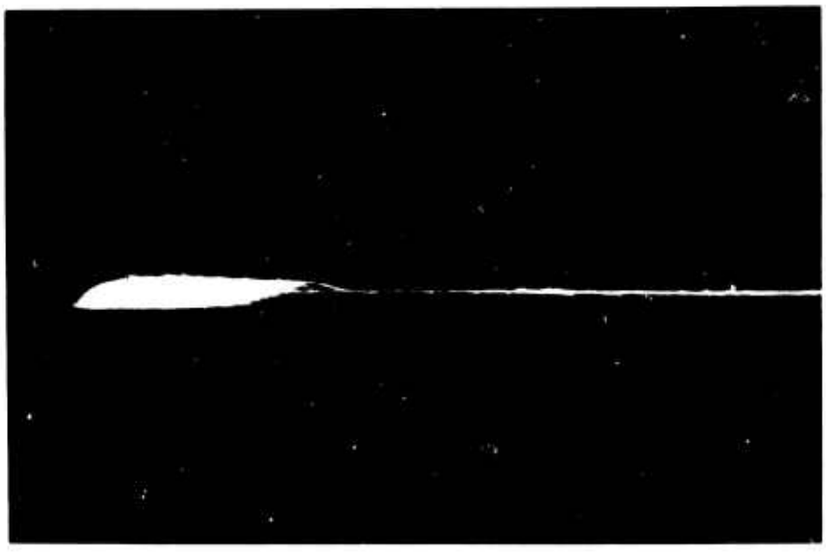

Figure 18. Tip-Vortex Flow Visualization from Top View as Shown by Helium-Bubble Technique for m_i=0, α=10°, and V=100 fps

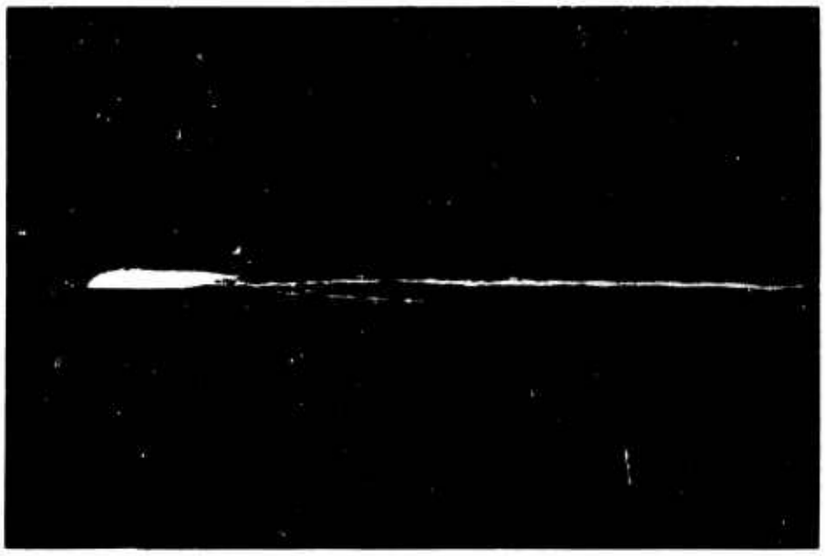

Figure 19. Tip-Vortex Flow Visualization from Top View as Shown by Helium-Bubble Technique for m_i=0.034 lb/sec, α=10°, and V=100 fps

Figure 20. Tip-Vortex Flow Visualization from Top View as Shown by Helium-Bubble Technique for m_i=0.062 lb/sec, α=10°, and V=100 fps

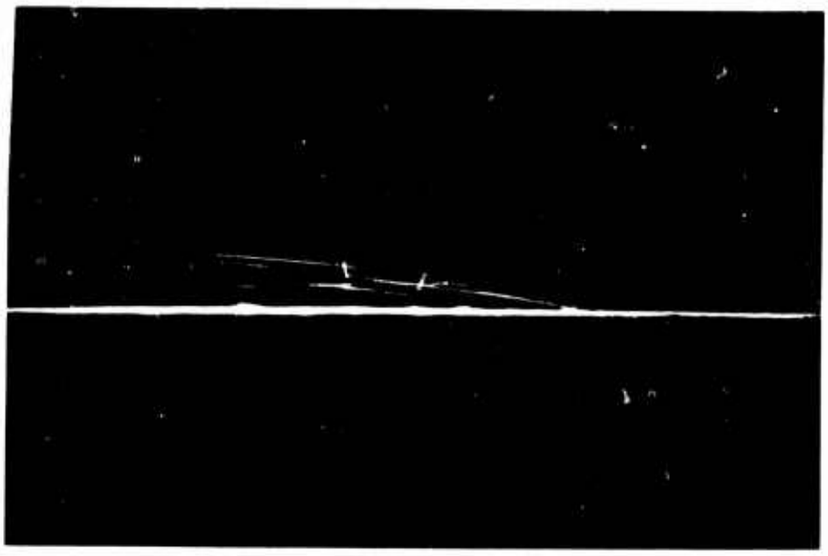

Figure 21. Tip-Vortex Flow Visualization at 12 Chordlengths Downstream as Shown by Helium-Bubble Technique for m_i=0 lb/sec, α=10°, and V=100 fps

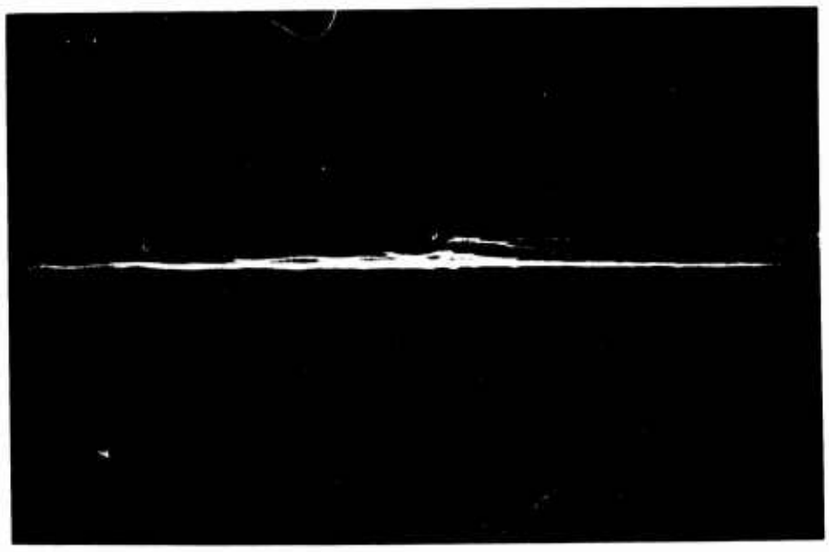

Figure 22. Tip-Vortex Flow Visualization at 12 Chordlengths Downstream as Shown by Helium-Bubble Technique for m_i=0.034 lb/sec, α=10°, and V=100 fps

Figure 23. Tip-Vortex Flow Visualization at 12 Chordlengths Downstream as Shown by Helium-Bubble Technique for m_i=0.062 lb/sec, α=10°, and V=100 fps

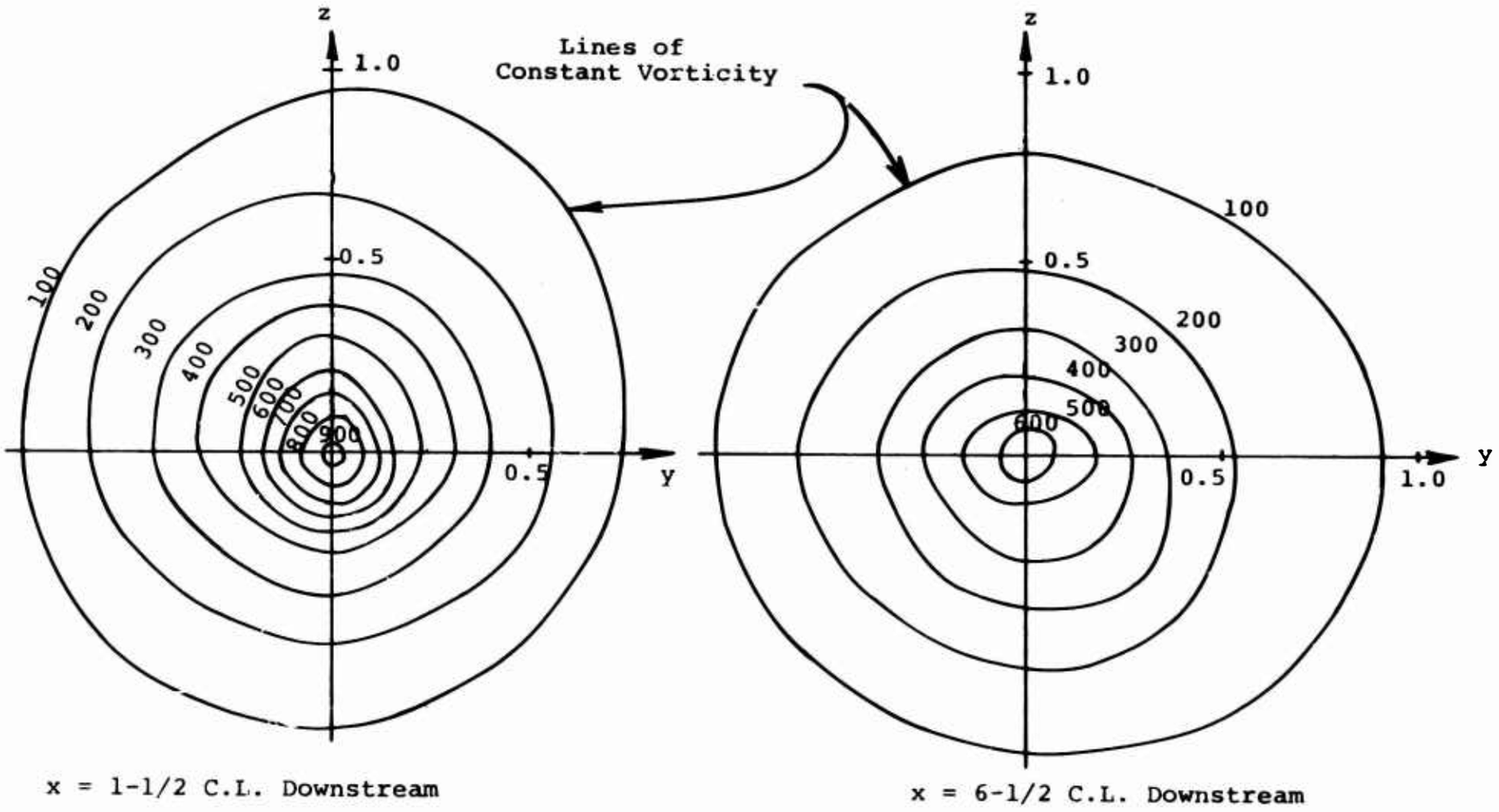

Figure 24. Contours of Constant Vorticity - V=200'/sec, α=10°, m_i=0.0 lb/sec

2.5:1 scale

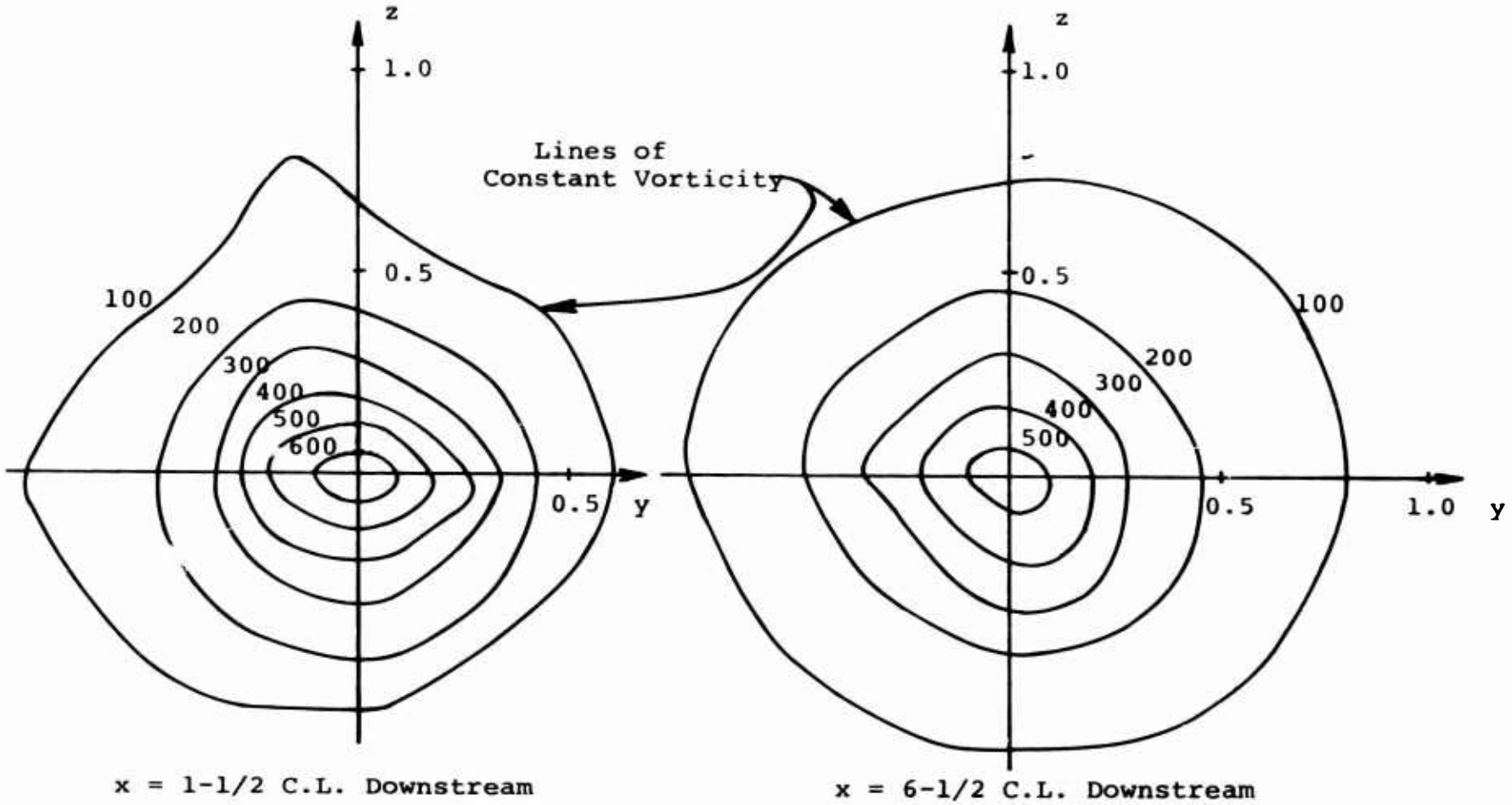

Figure 25. Contours of Constant Vorticity - V=200'/sec, α=10°, m_i=0.062 lb/sec

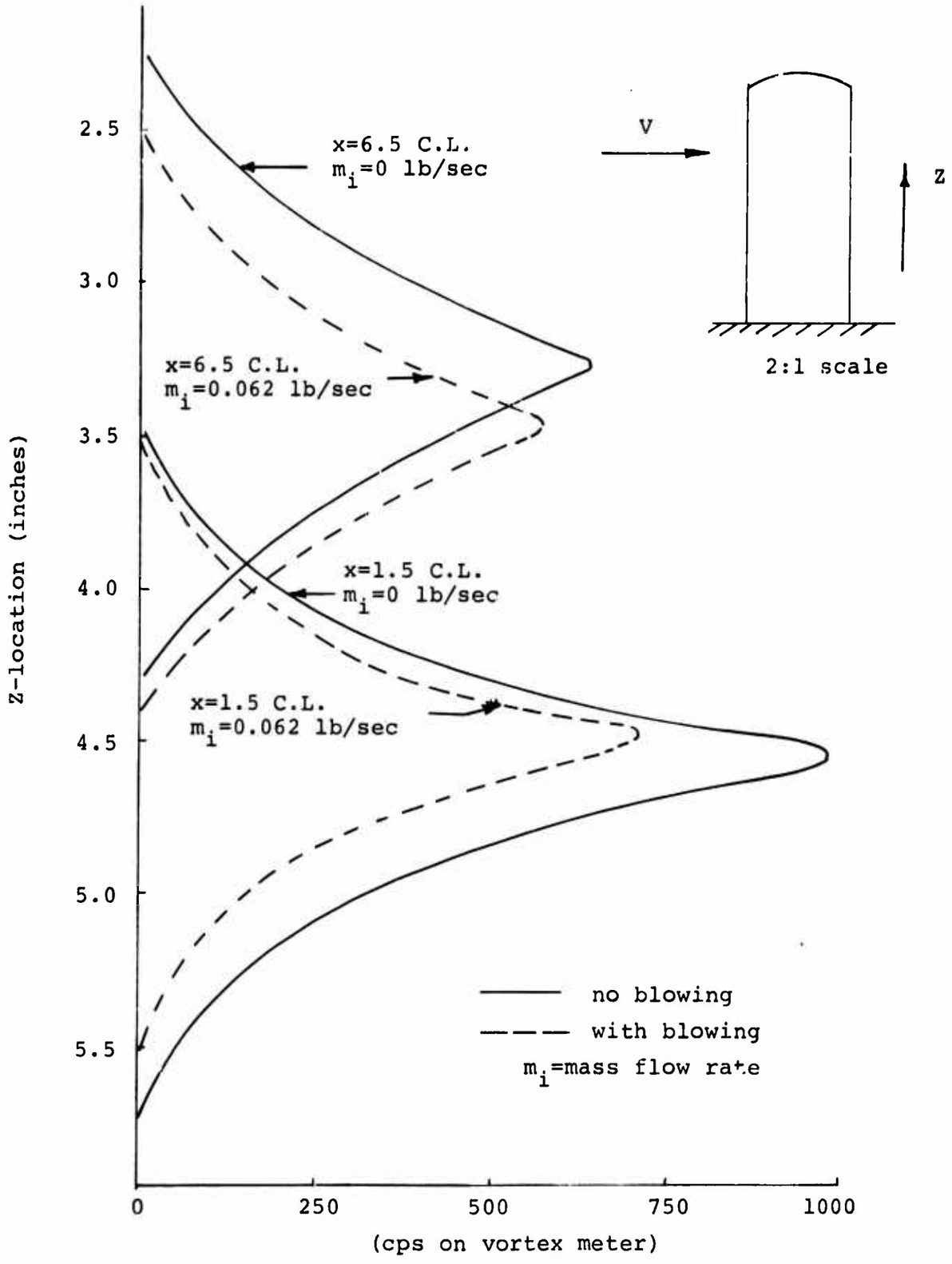

Figure 26. Vorticity Distribution Through Tip Vortex Core for m_i=0.0 and 0.062 lb/sec, α=10°, and V=200 ft per sec.

2.5:1 Scale

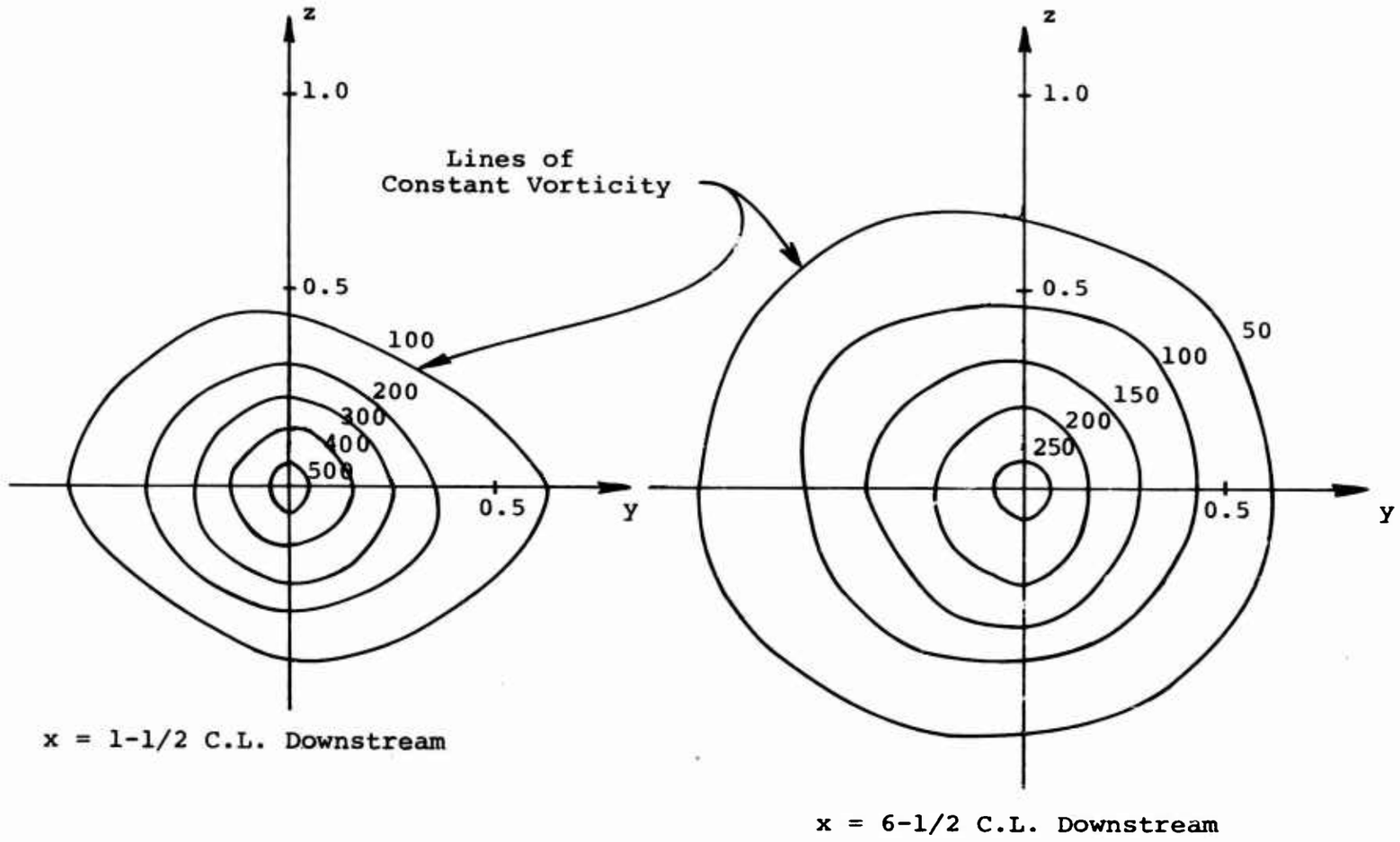

Figure 27. Contours of Constant Vorticity - V=200'/sec, α=10°, m_i=0.091 lb/sec

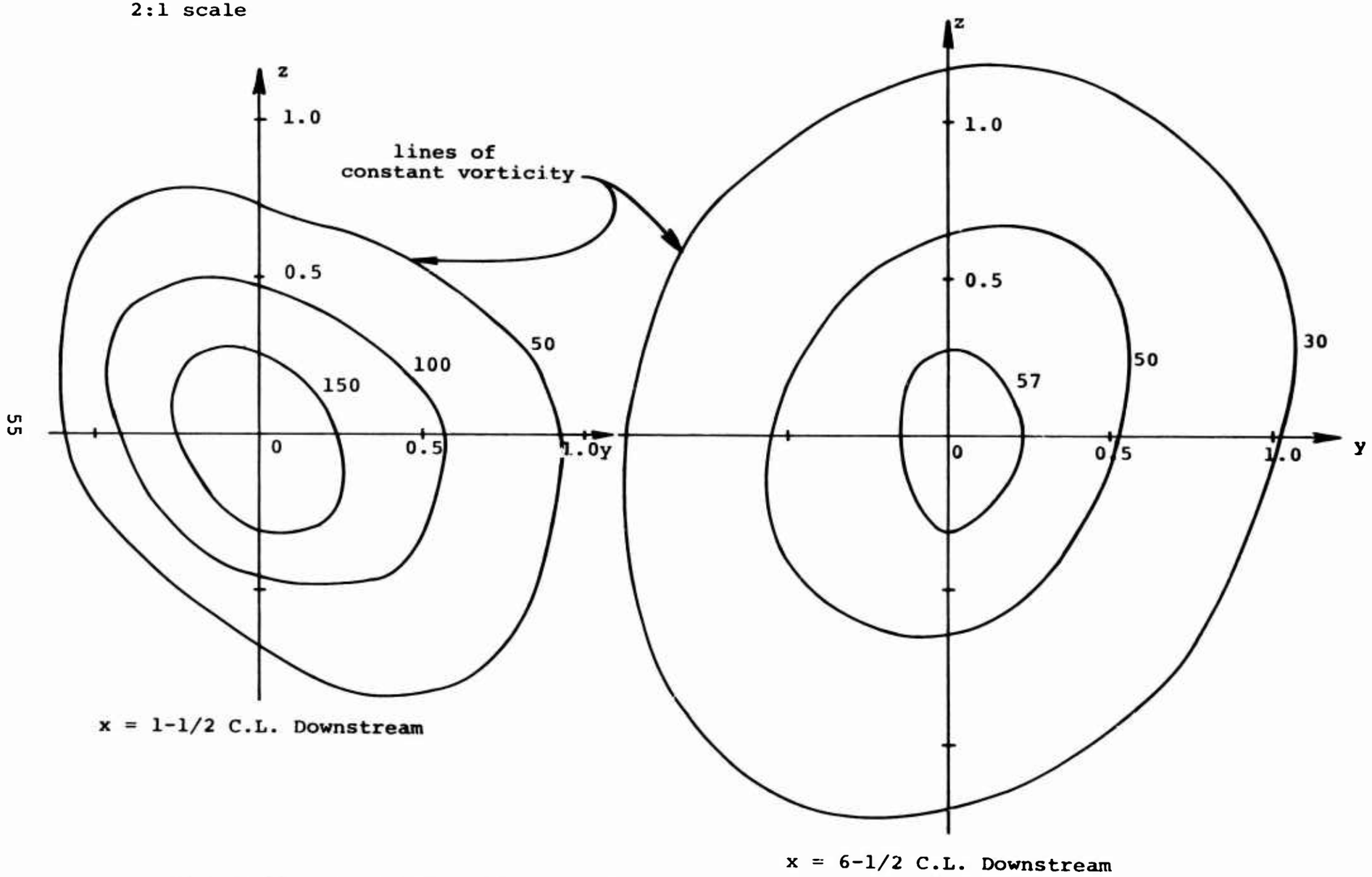

Figure 28. Contours of Constant Vorticity - V=200'/sec, α=10°, m_i=0.146 lb/sec

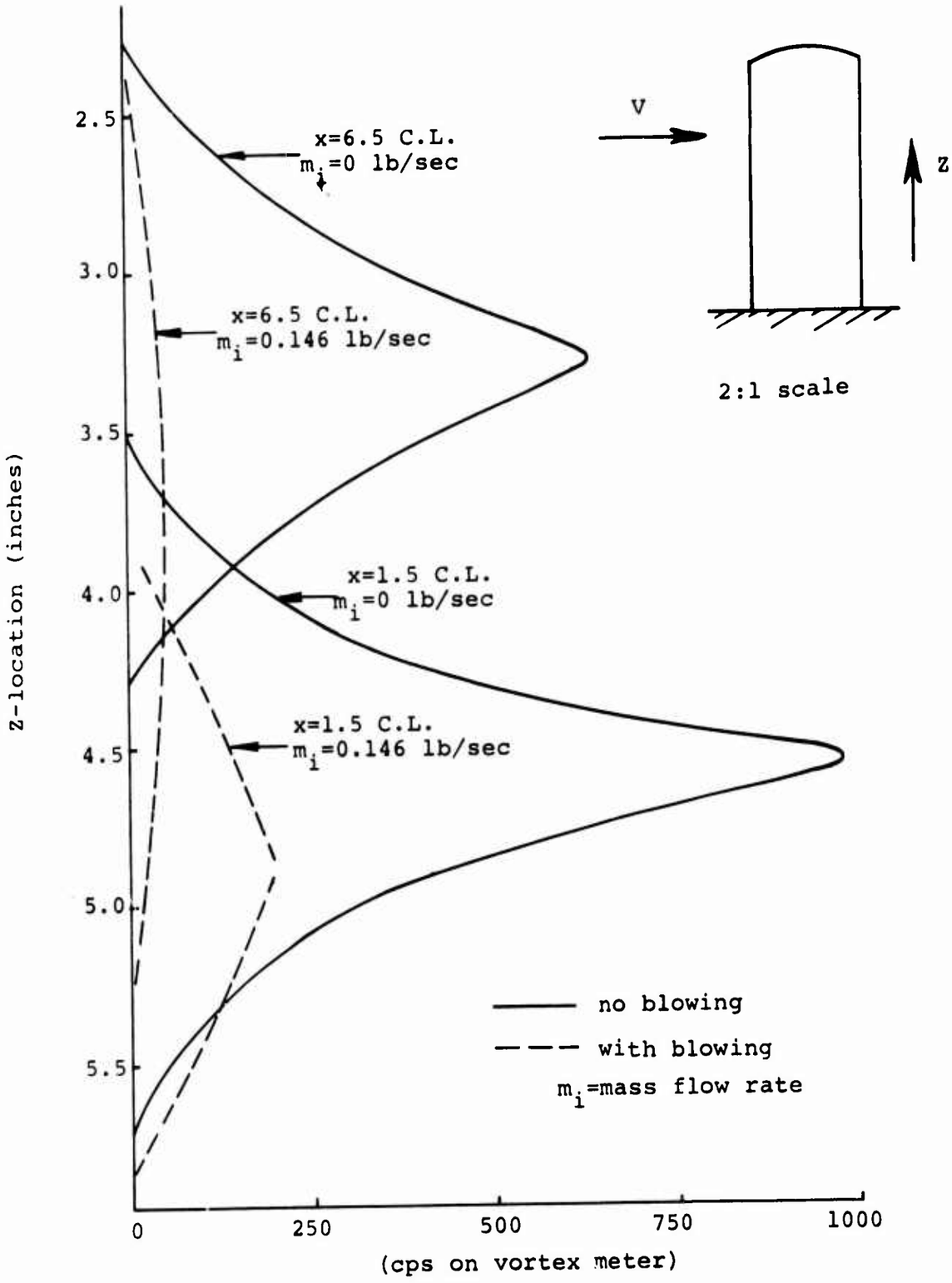

Figure 29. Vorticity Distribution Through Tip Vortex Core for m_i=0.0 and 0.146 lb/sec, α=10°, and V=200 ft per sec

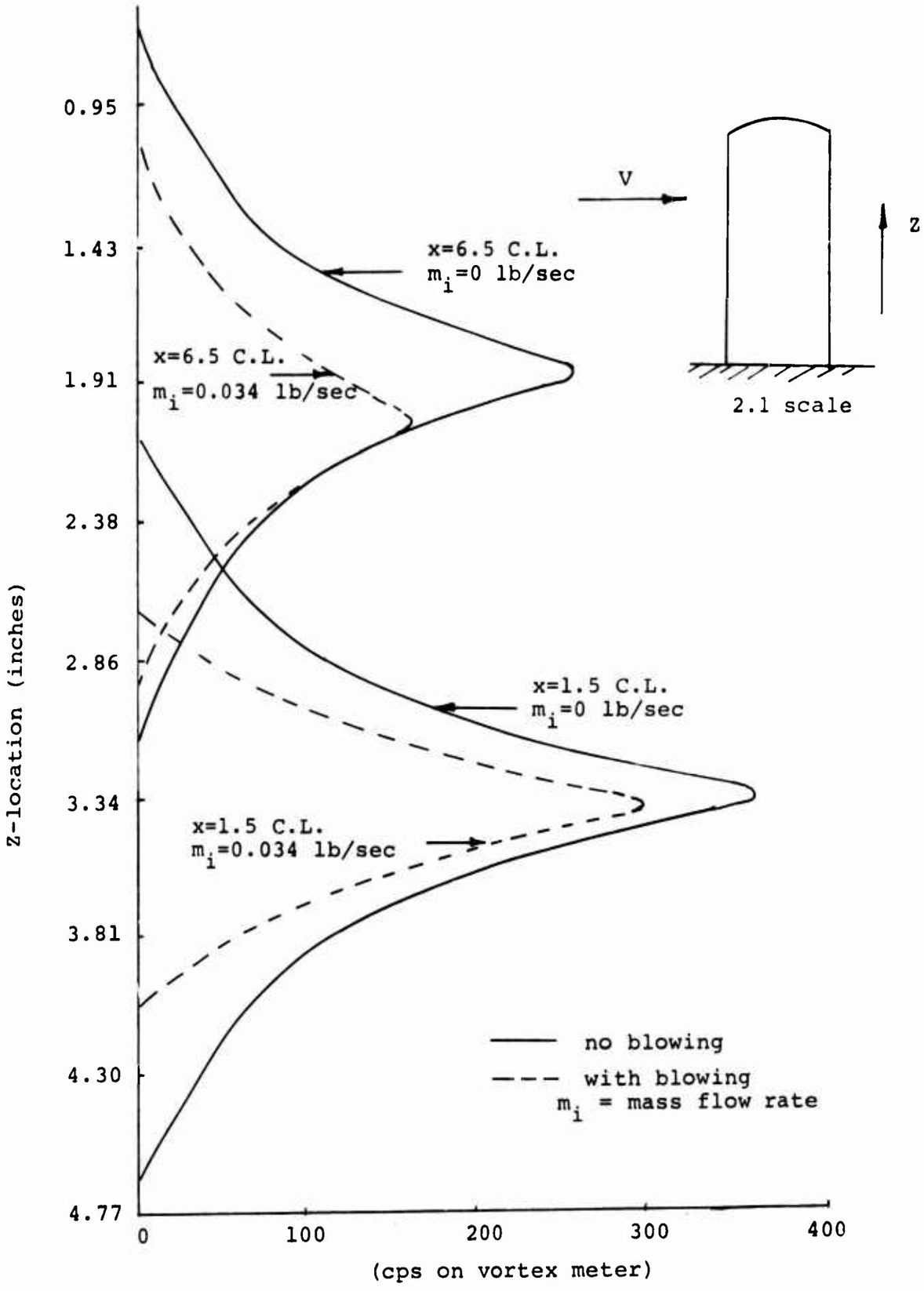

Figure 30. Vorticity Distribution Through Tip Vortex Core for m_i=0.0 and 0.034 lb/sec, α=10°, and V=100 ft per sec

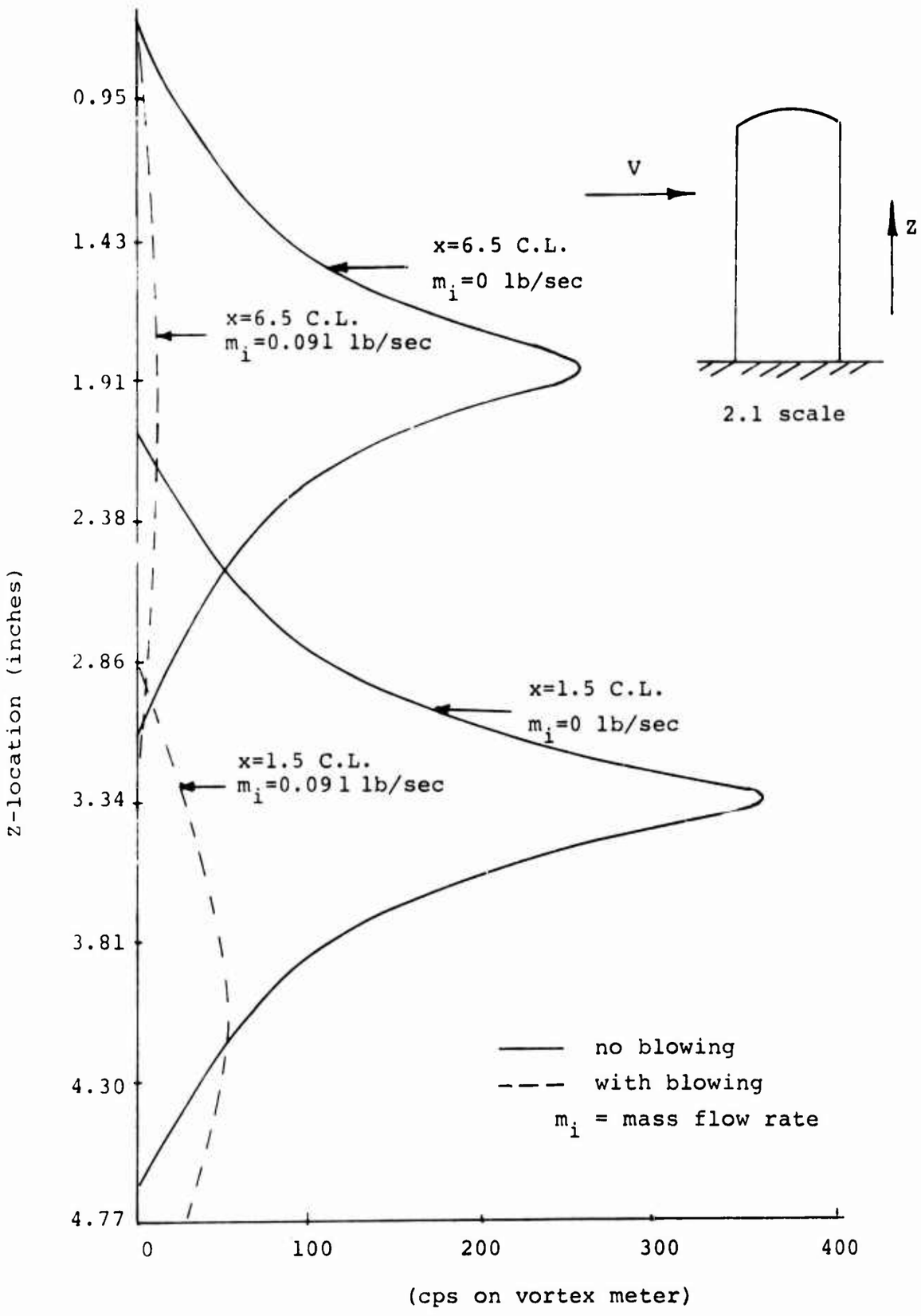

Figure 31. Vorticity Distribution Through Tip Vortex Core for m_i=0.0 and 0.091 lb/sec, α=10°, and V=100 ft per sec

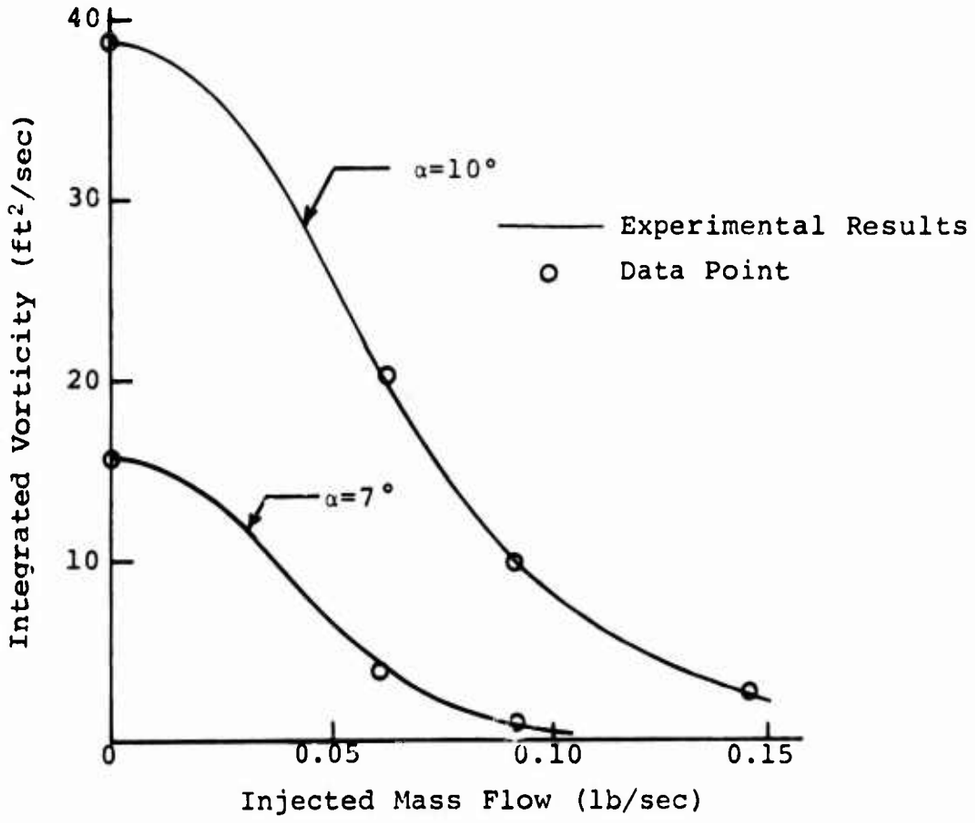

Figure 32. Measured Integrated Vorticity vs. Injected Mass Flow, V=200 fps at 6-1/2 Chordlengths Downstream

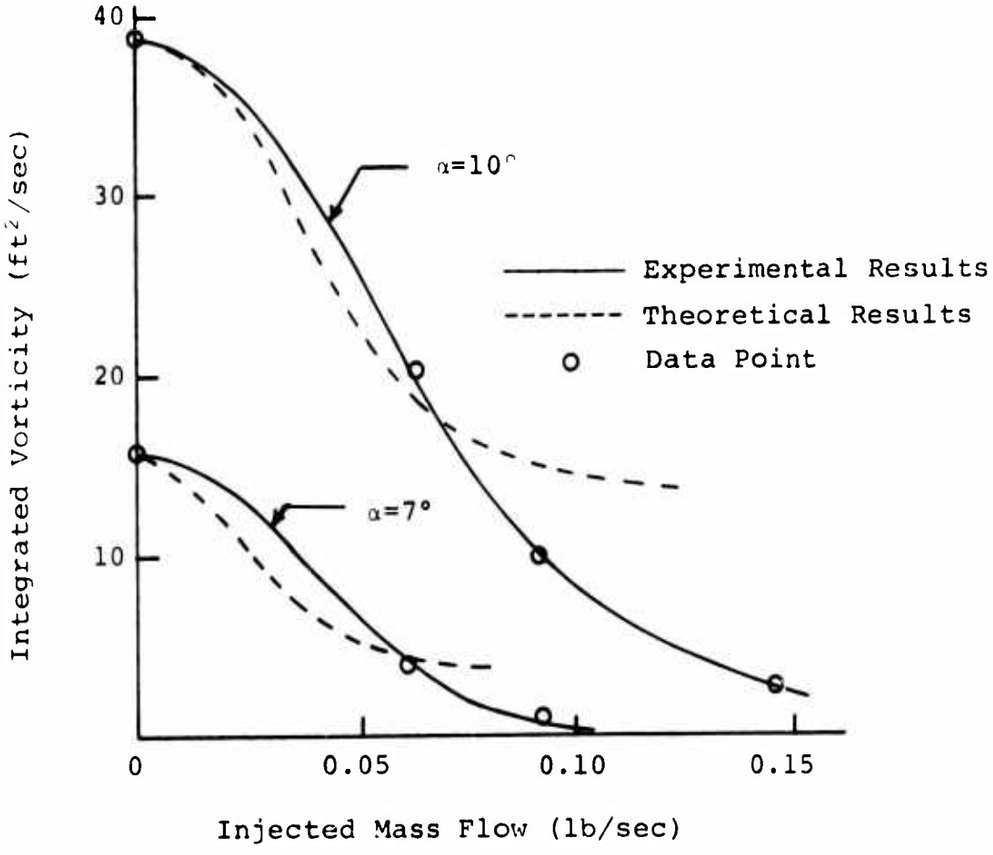

Figure 33. Comparison of Theory and Measured Integrated Vorticity vs. Injected Mass Flow, V=200 fps at 6-1/2 Chordlengths Downstream

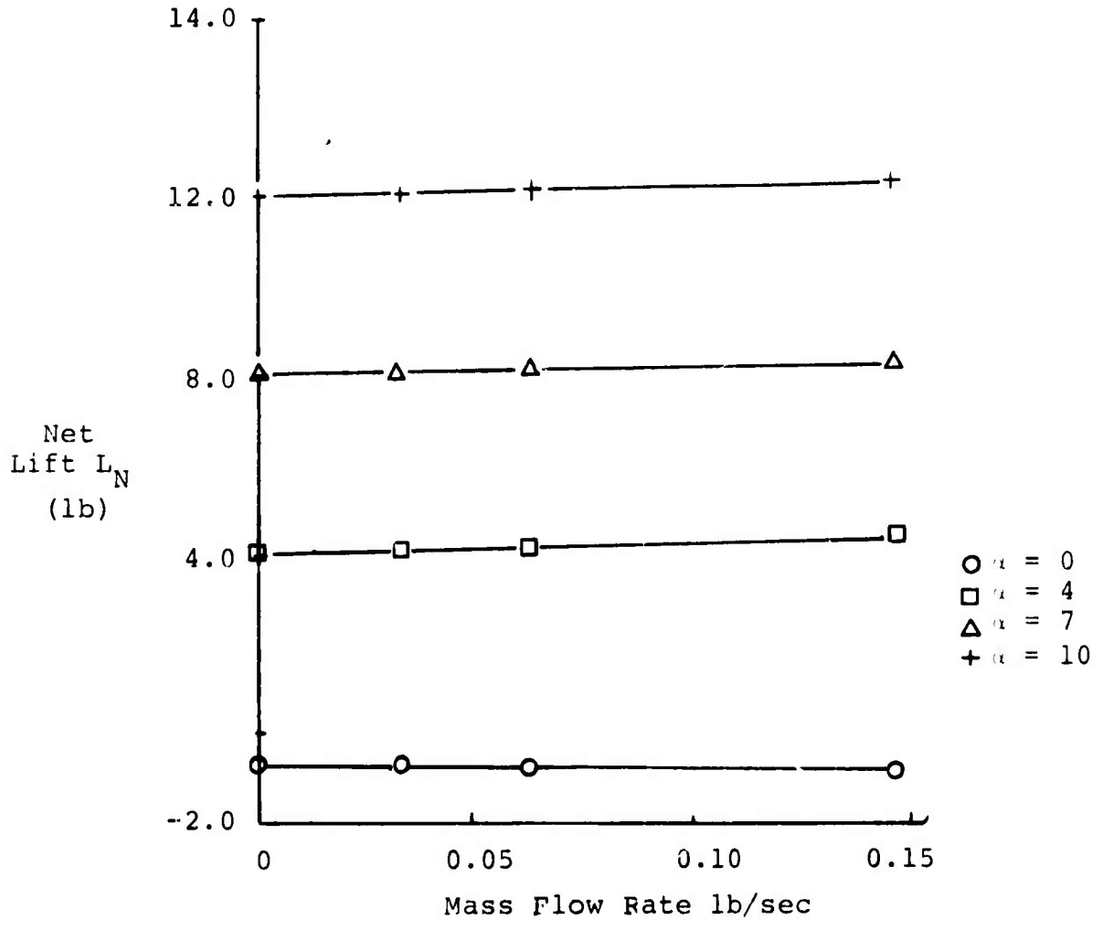

Figure 34. Experimental Lift Versus Injected Mass Flow Rate (m_i) lb/sec, V=100 ft per sec

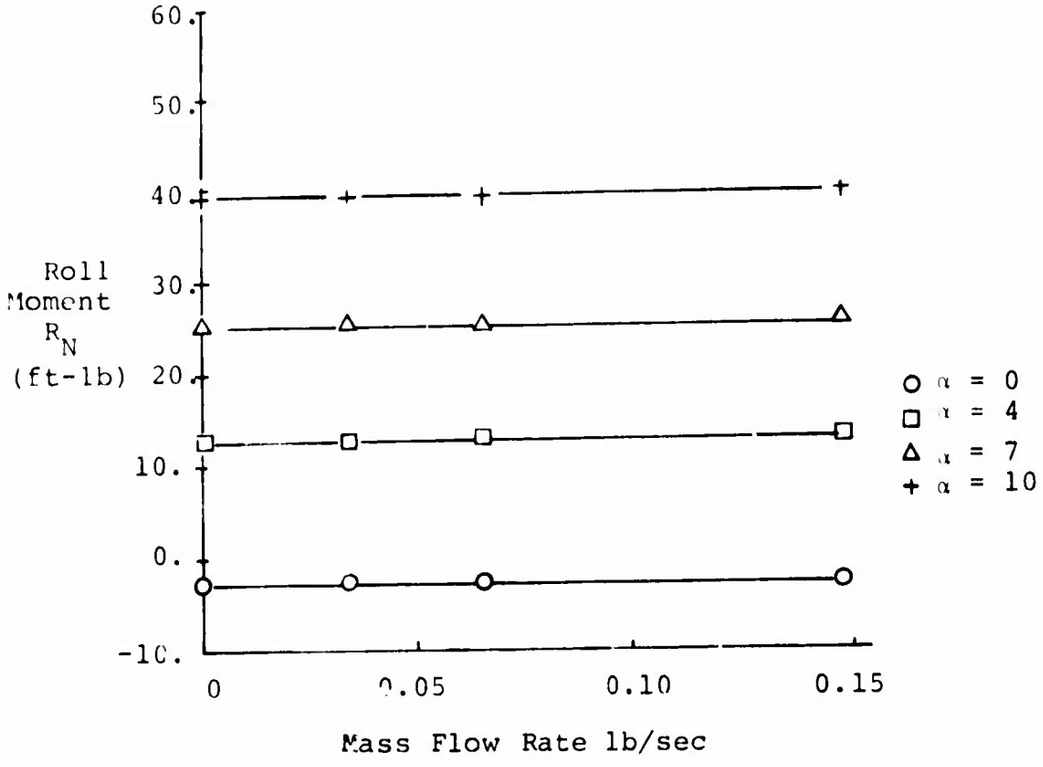

Figure 35. Experimental Roll Moment Versus Injected Mass Flow Rate (m_i) lb/sec, V=100 ft per sec

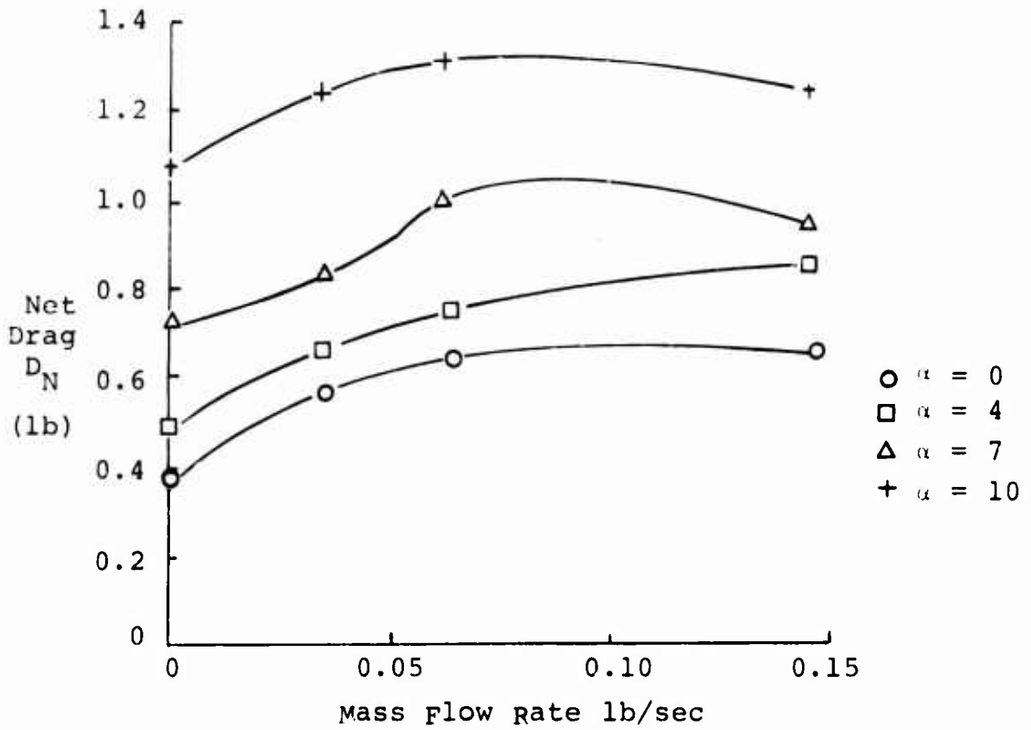

Figure 36. Experimental Drag Versus Mass Flow Rate, V=100 fps

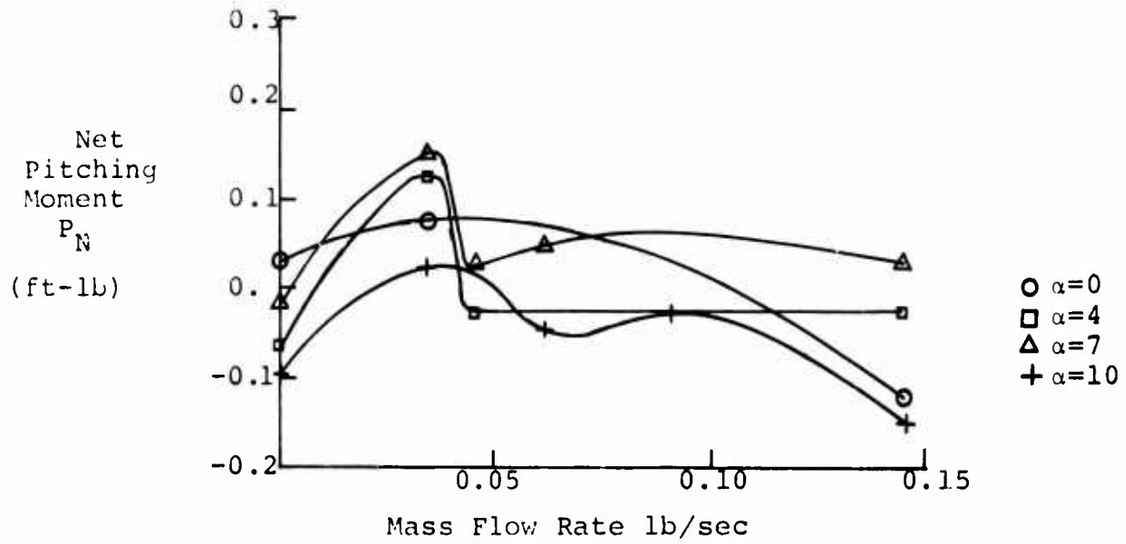

Figure 37. Experimental Pitching Moment Versus Injected Mass Flow Rate, V=100 fps

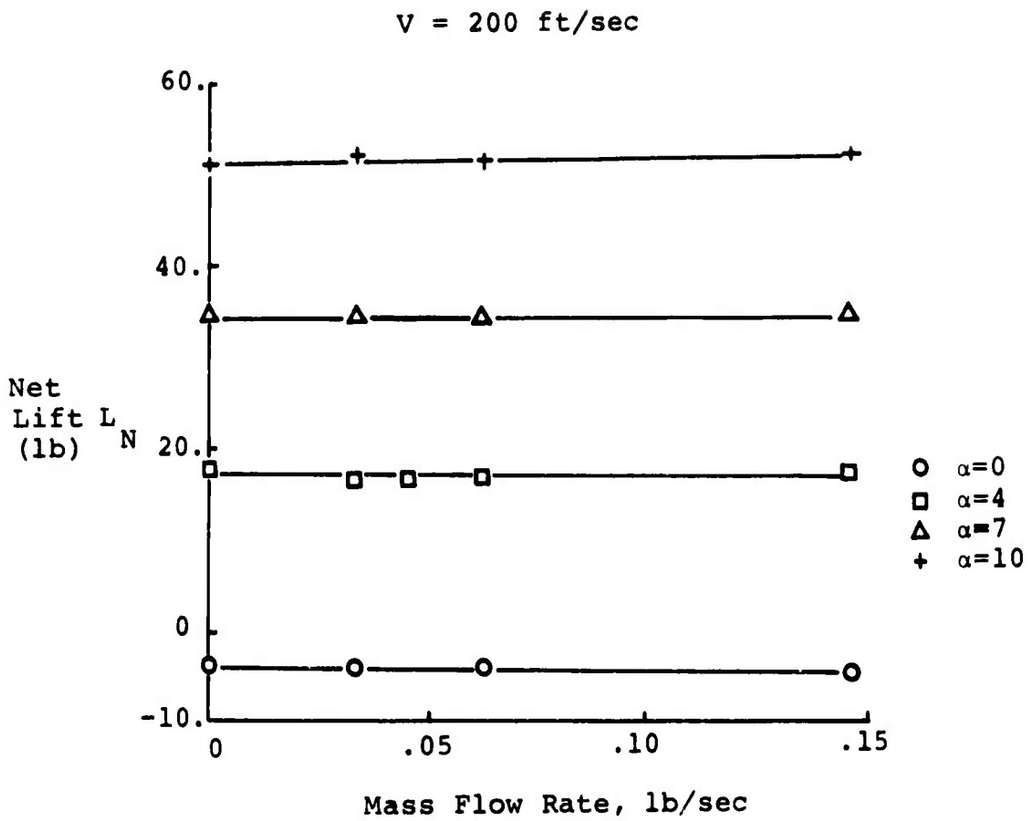

Figure 38. Experimental Lift Versus Injected Mass Flow Rate (m_i) lb/sec, V=200 ft per sec

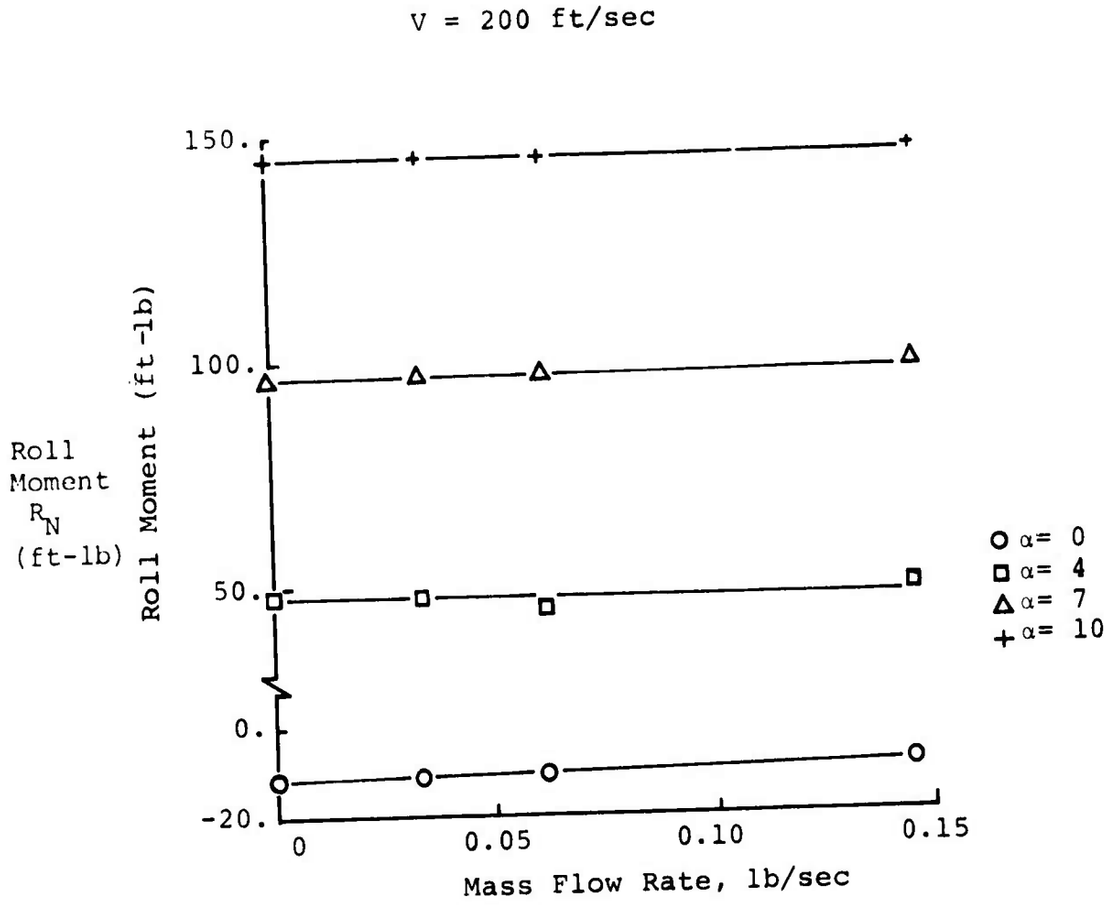

Figure 39. Experimental Roll Moment Versus Injected Mass Flow Rate (m_i) lb/sec, V=200 ft per sec

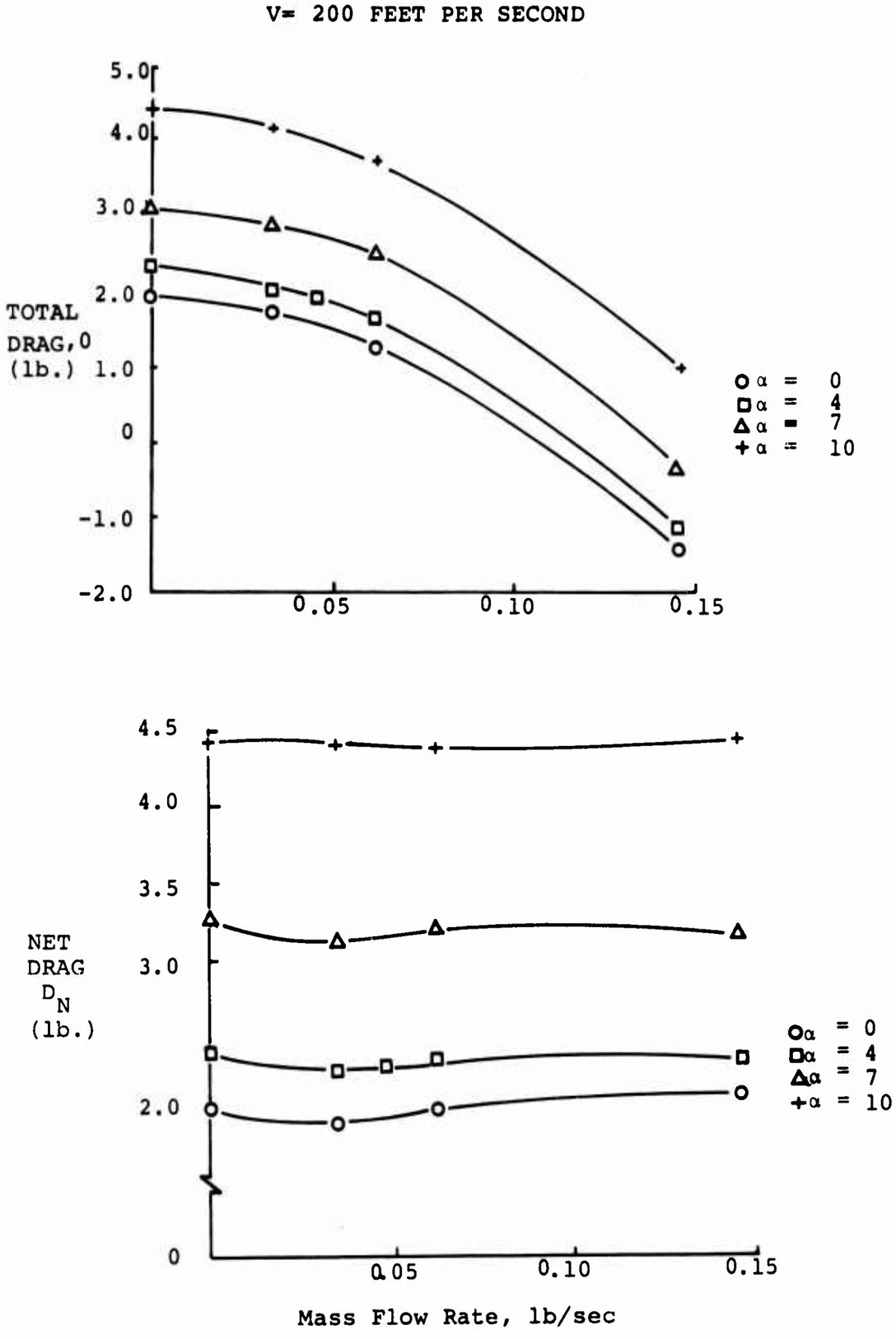

Figure 40. Experimental Drag Versus Injected Mass Flow Rate (m_j) lb/sec, V=200 ft per sec

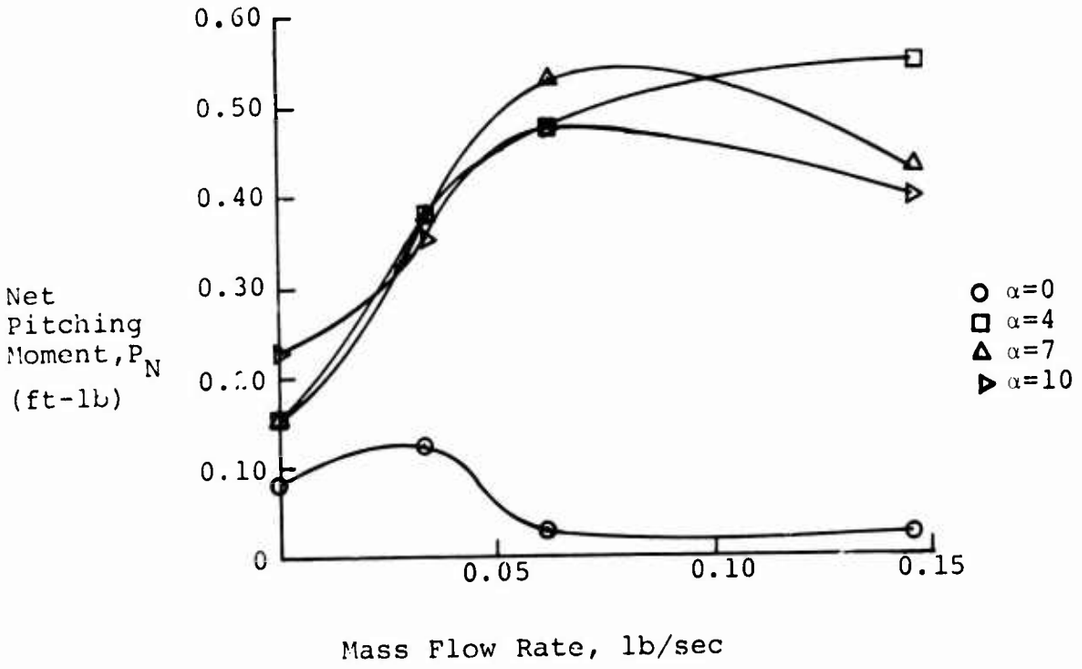

Figure 41. Experimental Pitching Moment Mass Flow Rate, V=200 fps

APPENDIX B

SUMMARY OF TABLES

TABLE I. SUMMARY OF TEST CONDITIONS FOR VORTEX-METER DATA

Model Angle of Attack (deg)	Air Mass Injection Rate (lb/sec)	Streamwise Position of Vortex-Meter (chordlengths behind trailing edge)	Tunnel Test Velocity (fps)
4	0 0.014 0.034 0.0455	1.5	100
7	0 0.034 0.0455 0.062	1.5	100
10	0 0.034 0.0455 0.062 0.091	1.5	100
4	0 0.014 0.034 0.0455	6.5	100
7	0 0.034 0.0455 0.062	6.5	100
10	0 0.034 0.0455 0.062 0.091	6.5	100

Model Angle of Attack (deg)	Air Mass Injection Rate (lb/sec)	Streamwise Position of Vortex-Meter (chordlengths behind trailing edge)	Tunnel Test Velocity (fps)
4	Data Not Obtained		200
7	0 0.062 0.091 0.146	1.5	200
10	0 0.062 0.091 0.146	1.5	200
4	0 0.034 0.0455 0.062	6.5	200
7	0 0.062 0.091 0.146		
10	0 0.062 0.091 0.146	6.5	200

TABLE II. MEASURED BALANCE DATA FOR V=100 FEET PER SECOND

α	m_i	Lift	Drag	Roll Moment	Drag Moment	Pitching Moment
0	0	-.85	0.36	-2.68	-1.43	0.03
0	0.034	-.80	0.55	-3.23	-2.23	0.08
0	0.146	-.85	0.64	-2.63	-1.50	-.13
4	0	4.10	0.46	12.75	-1.75	-.08
4	0.014	4.30	0.59	12.43	-2.65	+.04
4	0.034	4.20	0.64	12.65	-2.38	+.13
4	0.0455	4.35	0.69	12.55	-2.20	-.03
4	0.146	4.55	0.83	13.13	-2.13	-.03
7	0	8.15	0.70	25.1	-2.75	-.03
7	0.034	7.95	0.81	24.93	-2.45	+.15
7	0.0455	8.25	0.86	24.53	-2.73	+.03
7	0.062	8.25	0.98	25.00	-2.78	+.05
7	0.146	8.50	0.91	25.65	-2.73	+.03
10	0	12.40	1.05	39.1	-3.23	-.1
10	0.034	12.60	1.21	39.23	-3.80	+.03
10	0.062	12.70	1.29	39.45	-3.68	-.05
10	0.091	12.70	1.28	39.60	-3.38	-.03
10	0.146	12.90	1.21	40.25	-3.35	-.15

Tares

α	m_i	Lift	Drag	Roll Moment	Drag Moment	Pitching Moment
0	0.034	-.05	-.39	+.08	+.70	0
0	0.146	-.15	-3.70	-.65	+4.85	+.13
4	0.014	-.10	-.14	-.13	+.23	-.15
4	0.034	0	-.39	-.03	+.48	-.08
4	0.0455	0	-.58	+.38	+.80	+.15
4	0.146	+.10	-3.71	+.28	+5.28	+.10
7	0.034	0	-.40	+.03	+.28	-.08
7	0.0455	0	-.53	+.28	+.45	+.05
7	0.062	0	-.90	+.28	+1.20	+.03
7	0.146	+.255	-3.66	+.58	+5.30	+.08
10	0.034	-.10	-.36	+.23	+.38	-.03
10	0.062	+.10	-.90	+.48	+1.20	0
10	0.091	+.20	-1.60	+.43	+1.78	-.05
10	0.146	+.40	-3.59	+.58	+5.03	+.03

TABLE III. MEASURED BALANCE DATA FOR V=200 FEET PER SECOND

α	m_i	Lift	Drag	Roll Moment	Drag Moment	Pitching Moment
0	0	-4.0	1.99	-10.8	-6.93	0.08
0	0.034	-3.9	1.89	-10.4	-6.25	0.13
0	0.062	-3.9	1.98	-10.3	-6.73	0.03
0	0.146	-4.3	2.06	-8.3	-7.28	0.03
4	0	17.6	2.35	48.2	-8.30	0.15
4	0.034	16.6	2.21	48.8	-7.30	0.38
4	0.0455	16.9	2.26	0	0	0
4	0.062	17.0	2.30	45.9	-7.45	0.48
4	0.146	17.3	2.28	50.0	-7.38	0.55
7	0	34.5	3.23	96.7	-10.65	0.15
7	0.034	34.6	3.09	97.2	-9.85	0.38
7	0.062	34.2	3.19	97.1	-10.13	0.53
7	0.146	34.9	3.11	98.5	-9.85	0.43
10	0	51.3	4.43	144.4	-14.45	0.23
10	0.034	52.3	4.40	144.6	-13.90	0.35
10	0.062	52.1	4.36	145.7	-15.38	0.48
10	0.146	52.3	4.40	145.6	-13.85	0.40

Tares

α	m_i	Lift	Drag	Roll Moment	Drag Moment	Pitching Moment
0	0.034	-.2	-.16	-.20	0.10	0
0	0.062	-.2	-.70	-.35	1.33	-.05
0	0.146	-.4	-3.49	-.70	5.40	0
4	0.034	-.05	-.19	-.50	0.08	-.13
4	0.062	-.10	-.68	-.05	0.90	-.20
4	0.146	-.10	-3.45	-.55	5.35	-.13
7	0.034	-.10	-.20	+.18	0.30	-.05
7	0.062	-.10	-.68	+.20	0.90	-.10
7	0.146	+.1	-3.46	-.20	5.28	-.15
10	0.034	-.10	-.21	+.05	0.18	-.13
10	0.062	-.10	-.65	-.05	0.45	-.15
10	0.146	+.3	-3.41	+.38	5.20	-.15